Limiting and realistic efficiencies of multi-junction solar cells

Photonic Materials Group, FOM institute AMOLF, Amsterdam

Author: Hugo Doeleman

Supervisors: J. van de Groep and Prof. Dr. A. Polman

August 7, 2012

Abstract

In this study we used the detailed balance model to calculate efficiencies of multi-junction solar cells, varying the number of subcells, the concentration of solar light, the limiting angle for emitted light and the non-radiative recombination rate.

We first explain the detailed balance model and how it leads to the Shockley-Queisser formalism if one makes the assumption $E_g - qV_{oc} \gg kT$.

Using this model, limiting efficiencies for a solar cell with 1 to 8 junctions are obtained, assuming only blackbody radiative losses with both maximum concentration and no concentration. Optimal bandgap values are found. It is observed that using more than 5 junctions in a multi-junction cell offers only minimal gain in efficiency ($\sim 2\%$ efficiency per junction added).

Next, efficiencies for more realistic solar cells with 1-8 junctions are calculated, based on existing, abundant materials with bandgaps close to the optimum values that were found, and taking into account also non-radiative losses. It is found that concentration is a useful means to increase efficiency of the solar cell for any non-radiative recombination rate. However, the effect of angular restriction of emitted light becomes almost negligible ($\leq 2\%$ increase in efficiency) for more than 10 % of the recombination being non-radiative.

Finally, a detailed analysis of the single junction c-Si cell and the 5-junction Ge-(c-Si)-CZTS-(a-SiC)-GaP cell is performed. This shows that the former has a potential efficiency of 30.7 % for unconcentrated light and 38.3 % for a concentration of 1000 suns, and the latter has potentially 53.8 % efficiency for unconcentrated light and 64.5 % for a concentration of 1000 suns. The detailed insight into the contributions of loss processes solar cells that is provided in this study, is summarized in this last section and losses are compared and explained for these two particular cases.

Contents

1 Introduction

Contrary to intuition, a solar cell resembles a steam engine in more ways than one would suspect. Despite the obvious differences in appearance, applications and operation mechanism, both these energy conversion devices are ultimately limited in their efficiency by the same laws of thermodynamics. These laws can be applied to solar cells, the same as for any other energy conversion device, to obtain an upper limit on efficiency that is independent of most material parameters. It turns out that, just as for an old-fashioned steam engine, a solar cell is ultimately limited by the Carnot efficiency. Such a thermodynamic description of a solar cell can be very convenient when compared to conventional methods of modeling solar cell efficiencies, which employ material parameters such as carrier diffusion length and lifetimes, because it allows for a fast assessment of the cells performance.
Using a thermodynamical description employing energy and entropy exchanges, as was done by several authors, different expressions for limiting efficiencies can be obtained such as the Carnot limit (95%) or the Landsberg limit (93.3%), depending on which assumptions are made [1–3]. These models are very generic and can be applied to photovoltaic solar cells as well as e.g. photochemical, photothermal or photosynthetic convertors [4]. There is however also another model describing solar cell performance which is designed specifically for photovoltaic convertors: the detailed balance model. It does not employ energy and entropy exchange but the statistical balance of generation, extraction and recombination of charge carriers. It is however consistent with the thermodynamical approach, and can be shown to be equivalent [4, 5]. In this work, we will use the detailed balance model to calculate efficiencies of solar cells in various circumstances.

The detailed balance model has been known for over 50 years now, and has been used by many authors to model solar cell efficiencies. Shockley and Queisser were the first to use it for modeling a single junction solar cell, taking into account only radiative losses [6]. As new concepts for improving the efficiency of solar cells arose, other authors incorporated these into the model and studied their influences on solar cell efficiency. It was for instance conceived that concentrating solar light on a cell would improve efficiency, an effect that by now has been confirmed by experiments [5]. Multi-junction solar cells, cells consisting of multiple subcells, each with a bandgap optimized for a different part of the solar spectrum, have been thoroughly studied as well using the detailed balance model [2, 7–9]. More recently, the possibility of angular restriction, i.e. limiting the solid angle under which light emitted by the cell can exit the cell, was studied for its potential improvement of the efficiency of GaAs cells, taking into account also the contribution of non-radiative recombination [10, 11].

In this study, we systematically analyse the influence of all these effects simultaneously. The number of subcells in a multi-junction cell, the concentration of solar light, the limiting angle for emitted light and the non-radiative recombination rate are all varied and their effect on efficiency is studied. This provides detailed insight in the relative contribution of different loss processes in both single junction and multi-junction solar cells. On the basis of this analysis, materials are suggested for use in these solar cells. For these materials, the conditions are set that they must be abundant, non-toxic and obtainable in an economically feasible manner. Only in this way can the application of solar photovoltaic power generation ever be scaled to proportions suitable for supplying energy on a terawatt scale.
In the first part of this study, ideal efficiency limits were found for cells with 1 to 8 junctions by optimizing bandgap values, assuming only radiative recombination. Secondly,more realistic calculations of efficiency are performed for these cells, based on existing materials and including non-radiative recombination effects. Finally, two particular cases of solar cell configuration are studied more closely: the single junction c-Si cell and the 5-junction Ge-(c-Si)-CZTS-(a-SiC)-GaP cell. The different loss processes in single and multi-junction solar cells are compared and further explained through these two examples.

2 Theory

...every theoretical physicist who is any good knows six or seven different theoretical representations for exactly the same physics.
Richard Feynman

As is the case in so many fields of physics, the efficiency of a solar cell can be derived through completely different methods, as was mentioned above. One of those is the detailed balance model, which was first presented in 1961 by Shockley and Queisser, and it has been the standard model for calculating solar cell efficiencies ever since [6]. There are other models such as those based on energy and entropy exchange and those that employ the electron transport equations. However, the detailed balance model is usually preferred because it is relatively simple and insightful, and it requires much less extensive calculations than for example the more realistic models using the electron transport equations.

The detailed balance model is based on the statistical balance of electron-hole generation and recombination:

$$J_{out} = q(F_l - F_{rec}) \tag{1}$$

Here, J_{out} is the current that is extracted from the cell, F_l is the rate of generation of electron-hole pairs due to absorption of incident light, and F_{rec} is the total rate of carrier recombination, which is assumed to be at least partly radiative. q denotes the elementary charge. Note that all currents here are expressed in current per unit cell area. From this equation current voltage characteristics can be derived, as well as the efficiency of the solar cell.
Since the first version was presented in 1961, several authors have extended the detailed balance model [4, 12]. Their main contribution was to remove some approximations that lead to erroneous results in the case of large ratios of photo-generated current to dark current, for instance due to concentration of the sunlight. This has lead to the exact detailed balance model, which we shall discuss below. After this we shall show how from the exact model, one obtains the original model proposed by Shockley and Queisser by using the ideal diode approximation. Finally, the Shockley Quiser model will be adjusted for a multiple junction solar cell. However, first we will obtain an expression for the ultimate efficiency of a solar converter without using any current voltage characteristics. This will give us some insight in two of the principle fundamental losses in a solar cell; thermalization and loss of sub-bandgap light.

2.1 Ultimate Efficiency

In this section, the goal is to calculate the ultimate efficiency η_{ult} for a solar converter with a certain cut-off photon energy, in this case given by the bandgap energy E_g. It is based on the assumption that all photons with energy E larger than E_g are absorbed, and all photons with energy smaller than E_g are not. It is also assumed that each photon that is absorbed generates one electron-hole pair that is extracted at a voltage $V_g = \frac{E_g}{q}$. This implies that this solar converter has only two sources of loss: sub-bandgap light that is not absorbed and thermalization of high-energy carriers, which lose their excess energy above E_g. These losses are indicated in Fig. 1.

The efficiency of such a device is then given by the following expression:

$$\eta_{ult} = \frac{E_g Q_s(E_g)}{P_s} \tag{2}$$

$Q_s(E_g)$ is the number of photons in the solar spectrum with energy higher than or equal to the bandgap energy, that is $E \geq E_g$. P_s is the power of the solar irradiation, integrated over the full spectrum. Q_s and P_s can be expressed in the following way:

$$Q_s(E_g) = \int_{E_g}^{\infty} S(E)\, dE \tag{3}$$

$$P_s = \int_0^{\infty} E\, S(E)\, dE \tag{4}$$

$S(E)$ denotes the solar photon number spectrum, i.e. the incoming amount of photons in the solar irradiation on earth per m^2 per spectral unit. Several spectra have been used in various efficiency calculations in the

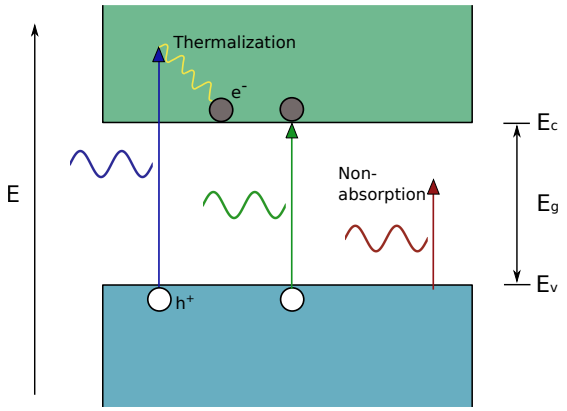

Figure 1: Loss processes that determine the ultimate efficiency of a solar converter with a cut-off frequency. High energy photons (blue) create carriers that thermalize, i.e. lose their excess energy. Photons with energies below the bandgap (red) cannot create free charge carriers, therefore they are not absorbed. e^- and h^+ denote electrons and holes, respectively. E_V, E_C and E_g indicate respectively valence band, conduction band and bandgap energies.

literature, such as the ideal blackbody spectrum for a blackbody at a temperature T=6000 °K [6], the AM0 spectrum or the AM1.5 spectrum [2, 4]. In this work, we shall use the AM1.5 spectrum.
η_{ult} has a maximum for a certain E_g, since the numerator in Eq. 2 vanishes for E_g approaching 0 as well as E_g approaching ∞. Indeed, as can be seen in Fig. 2, the maximum for η_{ult} lies at $E_g \approx 1.12$ eV.

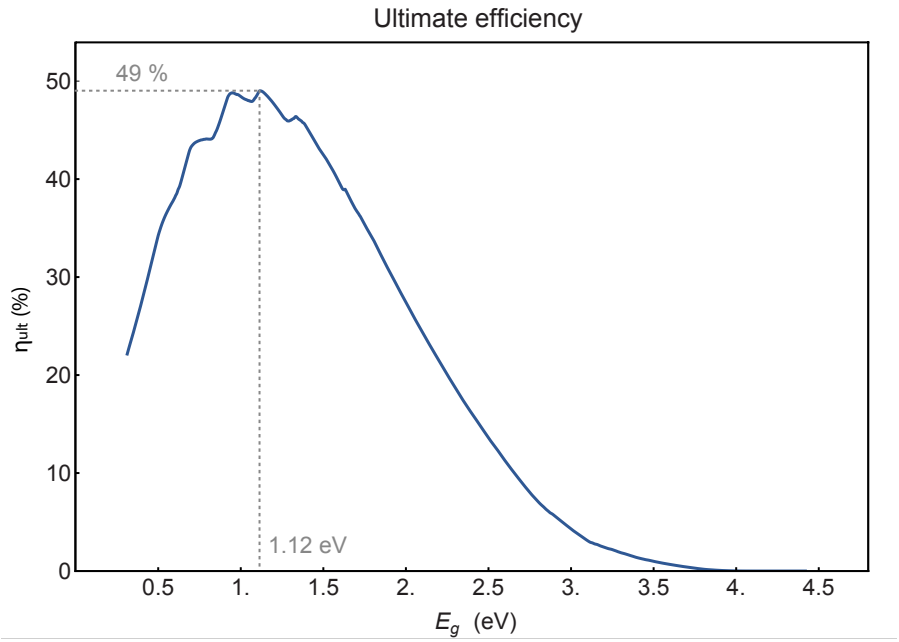

Figure 2: The ultimate efficiency for a single junction solar convertor as a function of its bandgap energy, under AM1.5 spectrum illumination. The maximum of 49 % occurs for a bandgap of 1.2 eV.

This ultimate efficiency is not an efficiency that a realistic solar cell could reach, since inevitable, fundamental losses will occur due to blackbody radiation from the cell. However, it will serve us as an absolute upper limit on the efficiency a the solar cell, which the efficiency obtained with a more realistic model cannot exceed. This is useful as a ward against computational errors.

2.2 The Exact Model

In this section, we will present a derivation from first principle of the exact detailed balance model, which predicts theoretical efficiencies for solar cells.

For the exact efficiency of a solar cell, consider again equation 1:

$$J_{out} = q(F_l - F_{rec}),$$

which is the starting point of our analysis. Carrier recombination rate F_{rec} and generation rate F_l shall be discussed below, after which an expression for the cell efficiency will be derived.

2.2.1 Carrier Recombination

The second term F_{rec} is the carrier recombination rate, which we assumed to be zero in the calculation of η_{ult}. It can be written here as:

$$F_{rec} = R_{rec}^{rad} + R_{rec}^{non-rad}, \tag{5}$$

with R_{rec}^{rad} and $R_{rec}^{non-rad}$ being the radiative and non-radiative recombination rate, respectively.

The radiative recombination rate originates from the cells blackbody radiation, more specifically it is the part of the cells blackbody spectrum that lies above the bandgap energy. For an emitter with emissivity t_c and a back reflector this is given as [3]:

$$R_{rec}^{rad} = t_c \frac{2\varepsilon_c}{c^2 h^3} \int_{E_g}^{\infty} \frac{E^2}{e^{(E-\mu)/kT_c} - 1}\, dE \tag{6}$$

Here ε_c denotes the étendue (per unit area) of the emitted radiation, which can be written as $\varepsilon_c = \pi\, sin^2(\theta_{lim})$. θ_{lim} refers to the maximum angle with respect to the vector normal to the cell surface under which radiation can be emitted. See appendix A for the derivation. c, h and k are the speed of light, the Planck constant and the Boltzmann constant respectively, and T_c is the cell temperature. μ corresponds to the chemical potential of the emitted photons, which is zero for a system in thermal equilibrium [7].[1]
However, a p-n junction solar cell under illumination is not in thermal equilibrium, and the photon chemical potential is equal to the separation of the electron and hole quasi-Fermi levels [7]. This can be understood by considering that the chemical potential is defined as the free energy brought to the system by the addition of a photon, other than the photon energy $h\nu$. This free energy comes from the relaxation of the carriers from their exited state, with which an energy is associated equal to the separation between the quasi-Fermi levels. This separation also equals qV, where V is the voltage over the cell [7]. We thus obtain the following expression for R_{rec}^{rad}:

$$R_{rec}^{rad} = t_c \frac{2\varepsilon_c}{c^2 h^3} \int_{E_g}^{\infty} \frac{E^2}{e^{(E-qV)/kT_c} - 1}\, dE \tag{7}$$

The non-radiative recombination rate $R_{rec}^{non-rad}$ is not easily obtained. Its origins compose of Auger recombination, bulk defect recombination and surface defect recombination. One can use an explicit expression to account for Auger recombination [10], or even an empirical expression for bulk defect and surface defect recombination [5], but this makes the analysis more complex and calculation time significantly longer. Moreover, the former two recombination types are device-dependent and therefore not relevant in the calculation of a theoretical upper limit to the efficiency.
In stead, we could use the external quantum efficiency (EQE) of radiative recombination to define the non-radiative recombination rate [10]. This macroscopic parameter that incorporates the contributions of all sources of non-radiative recombination is usually defined as the ratio between the fraction of the radiative recombination rate that escapes the cell and the total recombination rate. However, R_{rec}^{rad} can be varied by varying θ_{lim} or t_c, leading to a variation in EQE as well. We want to define a parameter describing the contribution of

[1] Note that if one sets μ to zero, assumes a perfect emitter ($t_c = 1$) and assumes that there is no mechanism that limits the angle of the outgoing blackbody radiation, i.e. $\theta_{lim} = 90°$ and $\varepsilon_c = \pi$, one obtains the usual expression for the blackbody radiation of temperature T_c, in units of W/m^2J.

non-radiative recombination that is independent of θ_{lim} and t_c, such that we can study these effects separately.[2] For this purpose, we define the parameter χ as the EQE for a cell with $t_c = 1$ and $\theta_{lim} = 90°$:

$$\chi \equiv \frac{R_{rec}^{rad,\,\pi,\,1}}{R_{rec}^{rad,\,\pi,\,1} + R_{rec}^{non-rad}}, \tag{8}$$

where $R_{rec}^{rad,\,\pi,\,1}$ is the radiative recombination rate for $t_c = 1$ and $\varepsilon_c = \pi$, that is $\theta_{lim} = 90°$.
$R_{rec}^{non-rad}$ is then:

$$\begin{aligned} R_{rec}^{non-rad} &= R_{rec}^{rad,\,\pi,\,1} \left(\frac{1-\chi}{\chi}\right) \\ &= \frac{\pi}{\varepsilon_c\, t_s}\, R_{rec}^{rad} \left(\frac{1-\chi}{\chi}\right) \end{aligned} \tag{9}$$

2.2.2 Carrier Generation

The first term on the right side of Eq. 1, F_l, is the rate of generation of carriers due to the absorption of incident light and is given by:[3]

$$F_l(E_g) = t_s\, C\, Q_s(E_g) \tag{10}$$

t_s is the probability that an incoming photon with $E \geq E_g$ creates an electron-hole pair, and depends on the reflectivity of the cell, the absorption coefficient of the material and light trapping in the cell. In this work we shall not consider the effect of these parameters, so we shall set t_s to unity. This can be realized in practice by using state of the art antireflection coatings [13] and a cell that is sufficiently thick or employs effective light trapping [14].
C denotes the concentration factor of the sunlight, and is a dimensionless quantity. C is 1 for unconcentrated sunlight under normal incidence, and has a maximum value of ~ 46000. This maximum is given by the ratio of the maximum étendue of light falling on a planar surface (π) and the étendue of the sunlight on earth. For sunlight under normal incidence, the latter is given by (in analogy with Eq. 36):

$$\varepsilon_s = \pi sin^2(\theta_s) \qquad \text{with} \qquad \theta_s = arcsin\left(\frac{R_{sun}}{D_{sun}}\right)$$

so that

$$\varepsilon_s = \pi \frac{R_{sun}^2}{D_{sun}^2} \tag{11}$$

Here, θ_s denotes the angle that the edge of the sun makes with the normal vector to the surface of the solar cell, analogues to θ_{lim} for emitted light. R_{sun} and D_{sun} are the radius of the sun and the distance between the earth and the sun, respectively. C_{max} is then:

$$C_{max} = \frac{\pi}{\varepsilon_{sun}} \quad = \frac{D_{sun}^2}{R_{sun}^2} \quad \approx 46000, \tag{12}$$

i.e. a concentration of 46000 suns. Finally, Q_s is the number of photons in the solar spectrum with energy higher than or equal to the bandgap energy, as given by Eq. 3.

2.2.3 Efficiency

With this information on the carrier generation and recombination, we can now set out to derive an expression for the efficiency of the cell. The incoming power P_s per unit area on the solar cell is given by Eq. 4. The

[2] A parameter that satisfies this condition and that is commonly used in previous studies [10, 15], is the internal quantum efficiency (IQE). However, to correctly link IQE to EQE, as is done by Kosten et al., knowledge of material parameters such as absorption coefficient, thickness and refractive index is required. These are parameters that we want to avoid in this work, because our results should be independent of material choice.

[3] One could also add a third term to the right side of eq. 1, to account for the incident background radiation, as some authors have done [4]. This can be an important contribution for a solar cell under diffuse illumination, but we do not consider this case here. In our case, the background radiation could be modelled as blackbody radiation from a body at the same temperature as the cell, usually taken to be 300 °K, which is completely negligible compared to the solar illumination.

output power of the solar cell is defined as the product $J_{out}\,V$. The efficiency is then, according to Eq. 1, 5 and 9:

$$\begin{aligned}\eta &= \frac{V\,J_{out}}{P_s} \\ &= \frac{qV}{P_s}\left(F_l - R_{rec}^{rad} - R_{rec}^{non-rad}\right) \\ &= \frac{qV}{P_s}\left(F_l - R_{rec}^{rad}(1 + \frac{\pi}{\varepsilon_c\,t_c\,\chi} - \frac{\pi}{\varepsilon_c\,t_c})\right)\end{aligned} \tag{13}$$

To obtain the maximum efficiency of a cell with E_g given, η must be optimized by varying V.

Eq. 13 is an exact result and applies to all types of illumination spectra and concentration factors. It is however a laborious procedure to optimize η with respect to E_g using this model, particularly for multi-junction solar cells where multiple bandgaps need to be varied. It is therefore useful to make an assumption that greatly simplifies the calculation, as we shall discuss below.

2.3 The Original Shockley-Queisser Model

In this section we discuss how, starting from the exact model as described above, one obtains the original detailed balance model as it was presented by Shockley and Queisser [6]. Although this model does not predict exact efficiencies under all circumstances, its advantage is that the calculation that is required to produce an efficiency is simpler and shorter.
In the first section we derive the ideal diode equation, starting from the exact model and taking an approximation valid for low cell voltages. In the second and the third section, we use the ideal diode equation to obtain expressions for open circuit voltage V_{oc} and fill factor FF, respectively. In the last section, we present the expression for efficiency that emerges from the Shockley-Queisser model and includes V_{oc} and FF.

2.3.1 The Ideal Diode Equation

Here we derive the ideal diode equation. If one makes the assumption that cell voltage never approaches the bandgap energy E_g, that is:

$$E_g - qV \gg kT_c, \tag{14}$$

R_{rec}^{rad} (Eq. 7) can be rewritten as:

$$\begin{aligned}R_{rec}^{rad} &\cong t_c\frac{2\varepsilon_c}{c^2h^3}\int_{E_g}^{\infty}\frac{E^2}{e^{(E-qV)/kT_c}}\,dE \\ &= t_c\frac{2\varepsilon_c}{c^2h^3}\int_{E_g}^{\infty}\frac{E^2}{e^{E/kT_c}}\,dE\,e^{\frac{qV}{kT_c}} \\ &= R_0^{rad}(t_c,\varepsilon_c,E_g)\,e^{\frac{qV}{kT_c}},\end{aligned} \tag{15}$$

with

$$R_0^{rad}(t_c,\varepsilon_c,E_g) = t_c\frac{2\varepsilon_c}{c^2h^3}\int_{E_g}^{\infty}\frac{E^2}{e^{E/kT_c}}\,dE \tag{16}$$

Here, $q\,R_0^{rad}(t_c,\varepsilon_c,E_g)$ denotes the dark current J_0 in the cell in the case that there is only radiative recombination ($\chi = 1$).

The following current-voltage relation is then obtained from Eq. 1:

$$\begin{aligned}J_{out} &= q\left(F_l - R_{rec}^{rad} - R_{rec}^{non-rad}\right) \\ &= q\left(F_l - R_{rec}^{rad}(1 + \frac{\pi}{\varepsilon_c\,t_c\,\chi} - \frac{\pi}{\varepsilon_c\,t_c})\right) \\ &= q\left(F_l - R_0^{rad}(1 + \frac{\pi}{\varepsilon_c\,t_c\,\chi} - \frac{\pi}{\varepsilon_c\,t_c})\,e^{\frac{qV}{kT}}\right) \\ &= q\left(F_l - R_0^{tot}\,e^{\frac{qV}{kT_c}}\right)\end{aligned} \tag{17}$$

where

$$qR_0^{tot} = R_0^{rad}(1 + \frac{\pi}{\varepsilon_c\, t_c\, \chi} - \frac{\pi}{\varepsilon_c\, t_c}) \tag{18}$$

now represents the dark current J_0 in the cell, including the contribution of non-radiative recombination (for $\chi \neq 1$).

For this result, only the approximation in Eq. 14 was used. With the use of another approximation, it can be shown that this equation is equivalent to the ideal diode equation. Rewriting Eq. 17 as follows:

$$J_{out} = q\left((F_l - R_0^{tot}) - R_0^{tot}\,(e^{\frac{qV}{kT_c}} - 1)\right), \tag{19}$$

and recognizing that for all practical purposes, $F_l \gg R_0^{tot}$, we arrive at the familiar equation for an ideal diode under illumination:

$$\begin{aligned} J_{out} &= q\left(F_l - R_0^{tot}\,(e^{\frac{qV}{kT_c}} - 1)\right) \\ &= J_{sc} - J_0\,(e^{\frac{qV}{kT_c}} - 1), \end{aligned} \tag{20}$$

Where $J_{sc} = J_l$ is the light-generated current or short-circuit current and J_0 the dark current.

2.3.2 Open Circuit Voltage

Here we derive an expression for the open circuit voltage V_{oc}, using the ideal diode equation (Eq. 20). With the current-voltage relation of the cell given by the ideal diode equation, the open circuit voltage V_{oc} can be obtained by setting $J_{out} = 0$:

$$\begin{aligned} V_{oc} &= \frac{kT_c}{q}\ln(\frac{J_{sc}}{J_0} + 1) \\ &\cong \frac{kT_c}{q}\ln(\frac{J_{sc}}{J_0}) \end{aligned} \tag{21}$$

Using Eqs. 10 and 18 we can rewrite this as:

$$\begin{aligned} V_{oc} &= \frac{kT_c}{q}\ln\left(\frac{t_s\, C\, Q_s(E_g)}{R_0^{rad}(t_c, \varepsilon_c, E_g)\,(1 + \frac{\pi}{\varepsilon_c\, t_c\, \chi} - \frac{\pi}{\varepsilon_c\, t_c})}\right) \\ &= \frac{kT_c}{q}\ln\left(\frac{\varepsilon_s\, t_s\, C\, Q_s(E_g)}{t_c\, \varepsilon_c\, R_0^{rad}(1, \varepsilon_s, E_g)\,(1 + \frac{\pi}{\varepsilon_c\, t_c\, \chi} - \frac{\pi}{\varepsilon_c\, t_c})}\right) \\ &= \frac{kT_c}{q}\left\{\ln\left(\frac{Q_s(E_g)}{R_0^{rad}(1, \varepsilon_s, E_g)}\right) + \ln\left(\frac{C\,\varepsilon_s}{\varepsilon_c\, t_c + \frac{\pi}{\chi} - \pi}\right) + \ln(t_s)\right\} \end{aligned} \tag{22}$$

with $\varepsilon_s = \pi\left(\frac{R_{sun}}{D_{sun}}\right)^2 \cong 6.80 \cdot 10^{-5}$ denoting the étendue of the unconcentrated solar radiation.

For a cell under unconcentrated illumination, with maximum angular restriction of outgoing light (i.e. $\varepsilon_c = \varepsilon_s$), only radiative recombination ($\chi = 1$), unity emissivity and perfect absorption ($t_c = t_s = 1$), all terms but the first in Eq. 22 are zero. This corresponds to the maximum possible efficiency achievable by a solar cell. The second term in Eq. 22 can only be zero or negative, since the étendue of the outgoing light, ε_c, must be larger than or equal to $C\,\varepsilon_s$, the étendue of the incoming light. In other words, photons can always exit along the same path as they entered. The last term in Eq. 22 depends on the absorptivity and reflectivity of the cell. In this work, t_s and t_c are always set to unity, so this term vanishes.

2.3.3 Fill Factor

Here we use Eqs. 20 and 21 to derive an expression for the fill factor FF. The fill factor is defined as:

$$FF \equiv \frac{V_{max}\, J_{max}}{V_{oc}\, J_{sc}}, \tag{23}$$

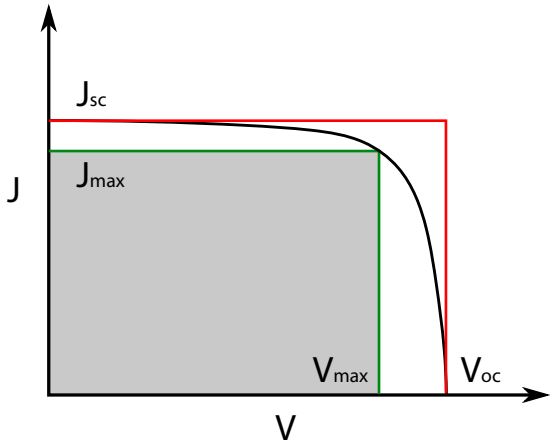

Figure 3: An example of a solar cell J-V characteristic, with V_{max} and J_{max} indicating respectively the voltage and current at maximum power point. V_{oc} and J_{sc} denote open circuit voltage and short circuit current, respectively. The fill factor is the shaded area subtended by the green box , divided over the area subtended by the red box.

with V_{max} and J_{max} the voltage and current at maximum power point, respectively. These are illustrated in Fig. 3.

By optimizing the output power

$$P_{out} = V \cdot J_{out}(V) \quad = V \left(J_{sc} - J_0 \left(e^{\frac{qV}{kT_c}} - 1 \right) \right) \tag{24}$$

with respect to voltage V, one obtains an expression for V_{max}. V_{max} is the solution to the equation:

$$\left(1 + \frac{qV_{max}}{kT_c} \right) e^{\frac{q}{kT_c}(V_{max} - V_{oc})} = 1 \tag{25}$$

With V_{max} given as a function of V_{oc} and T_c, J_{max} is given by eq. 17. This gives the following expression for the fill factor: [4]

$$FF = \frac{V_{max}}{V_{oc}} \left(1 - e^{-\frac{q}{kT_c}(V_{oc} - V_{max})} \right) \tag{26}$$

Note that, because V_{max} is a function of V_{oc} and T_c only, FF also depends only on V_{oc} and T_c, in the case of an ideal diode.

2.3.4 Efficiency

The efficiency of the solar cell is then given as:

$$\begin{aligned} \eta &= \frac{V_{max}\, J_{max}}{P_s} \\ &= FF\, \frac{V_{oc}\, J_{sc}}{P_s} \end{aligned} \tag{27}$$

This expression has a significant advantage over the exact solution in Eq. 13: no numerical optimization of η with respect to V is necessary. In stead, Eq. 27 gives the efficiency at maximum power point automatically, as this is captured in the factor FF.

For any solar cell under unconcentrated light with $\theta_{lim} = 90°$, the approximation in Eq. 14 is valid, so the ideal diode equation (Eq. 17) and the corresponding efficiency (Eq. 27) holds. On the other hand, for concentrated sunlight, or if $\chi \approx 1$ and θ_{lim} is very small, cell voltages may be almost as high as E_g/q, at which point the approximation breaks down. In appendix B, we show that despite this, efficiencies obtained using the ideal diode equation remain valid within a small error.

[4] In obtaining this expression, one makes the assumption that $exp\left[\frac{qV_{max}}{kT_c}\right] \gg 1$. This expression thus breaks down for high temperatures or small V_{max}, i.e. small E_g or weak illumination. For all our purposes however, Eq. 26 holds.

2.4 Multi-junction Solar cells

If we consider the case where we have a solar cell that consists not of a single p-n junction but of multiple junctions with different bandgaps that each absorb a different part of the solar spectrum, our expression for the efficiency should be slightly modified. The analysis is slightly different for cells with tandem geometry than for cells with a spectrum splitting device [7], but we shall only concern ourselves with the latter. Furthermore, we shall assume that the ideal diode approximation is valid, such that the single cell efficiency is correctly described by Eq. 27.

For the i-th subcell in a multi-junction solar cell with bandgap E_g^i, where $E_g^1 > E_g^2 > ... > E_g^i > ...$, the short circuit current is given by:

$$J_{sc}^i = q\, t_s\, C\, Q_s^i \tag{28}$$

where

$$Q_s^i = \int_{E_g^i}^{E_g^{i-1}} S(E)\, dE \tag{29}$$

This expression assumes that there is some perfect mechanism for splitting the solar spectrum, directing each part of the spectrum to the corresponding subcell without any losses.

The dark current is denoted by:

$$J_0^i = q\, R_0^{rad,i}(t_c, \varepsilon_c, E_g^i) \left(1 + \frac{\pi}{\varepsilon_c\, t_c\, \chi} - \frac{\pi}{\varepsilon_c\, t_c}\right) \tag{30}$$

with

$$R_0^{rad,i}(t_c, \varepsilon_c, E_g^i) = t_c \frac{2\varepsilon_c}{c^2 h^3} \int_{E_g^i}^{\infty} \frac{E^2}{e^{E/kT_c}}\, dE \tag{31}$$

in analogy with Eq. 16. We assume that C, $\mathrm{t_c}$, $\mathrm{t_s}$ and χ do not differ between the subcells. It is also implicitly assumed in Eq. 31 that the area of a subcell remains the same irrespective of the number of subcells.

Finally, with these expressions for J_{sc}^i and J_0^i the efficiency of the N-junction solar cell is:

$$\eta = \frac{1}{P_s} \quad \sum_{i=1}^{N} F F^i\, V_{oc}^i\, J_{sc}^i \tag{32}$$

3 Methods

In this work we have calculated the efficiencies of single and multiple junction solar cells using simulations in *Mathematica*, based on the Shockley-Queisser model presented in 2.3. The influence of four parameters on the efficiency of a solar cell was studied: The number of junctions, the concentration factor C, the limiting angle of emitted radiation θ_{lim} and the parameter χ. These studies can be separated in the following three parts:

- Calculation of the ideal efficiency limits of solar cells with 1 to 8 junctions by optimization of subcell bandgap energies.
- Calculation of more realistic efficiencies for single junction and multi-junction cells, based on existing, abundant materials with non-unity χ.
- A more detailed analysis of two particular solar cell configurations: The single junction c-Si cell and the 5-junction Ge-(c-Si)-CZTS-(a-SiC)-GaP cell.

In this section, we will discuss firstly the optimization procedure used in the first part. Secondly, criteria are set for the materials that were found in the second part on realistic efficiencies. Finally, we discuss the sources of uncertainty in the values for efficiency that were obtained.

In all simulations, emissivity t_c and absorptivity t_c are set to 1. We make use of Eq. 27 or, for multiple junction cells, Eq. 32 to calculate solar cell efficiencies. For the solar spectrum, the AM1.5 D spectrum is used.

For the design of a multi-junction solar cell, we take the spectrum splitter geometry. There exist currently two different designs for such a multi-junction solar cell: the tandem cell geometry, where the different subcells are stacked on top of each other, and the spectrum splitter geometry, where some spectrum splitting device distributes the light of different wavelengths to the subcells [7,15]. The first design requires the materials to be epitaxially grown on top of each other. This severely constraints the choice of materials and makes fabrication expensive. Also, because the subcells are connected in series, one has to match the currents of the subcells, which limits the efficiency. The spectrum splitter design has the advantage that the subcells are disconnected and can be operated individually, which means that one has full flexibility in the choice of materials, no current matching is necessary and fabrication can be less expensive.
Several spectrum splitter designs have been realized and have been demonstrated work in practice [16, 17]. In this work we shall not focus on the design of the spectrum splitter, merely on the efficiencies that can be obtained using its principles. Therefore it is assumed that the spectrum splitting occurs without losses.

3.1 Optimization Procedure for Ideal Efficiency Limits

In the first part of this work, we optimize bandgap values for solar cells with 1 to 8 junctions to find their maximum possible efficiencies. We take $\chi = 1$. Optimization occurs as follows.
Bandgap values of each subcell are varied in steps of 0.1 eV and cell efficiency is calculated for every combination of bandgaps $\left\{E_g^1, E_g^2, \ldots, E_g^N\right\}$. This gives us a maximum efficiency and corresponding optimum bandgap values. This optimum is then further refined by repeating the operation, varying the bandgaps E_g^i now in steps of 0.02 eV in the domain $\left[E_{g,opt}^i - 0.05\,\text{eV}\,,\, E_{g,opt}^i + 0.05\,\text{eV}\right]$, where $E_{g,opt}^i$ is the optimum value for the i-th bandgap as found by varying the bandgaps in steps of 0.1 eV. This method of optimization is illustrated in Fig. 4 for the case of the ultimate efficiency of a single junction cell.
In this way, optimum bandgap values and maximum efficiencies are found for:

1. The ultimate efficiency: η_{ult}
2. The efficiency under maximum concentration:[5] η_{Cmax}
3. The efficiency for no concentration or angular restriction: $\eta_{C=1}$

[5]Note that if $\chi = 1$, concentration is completely equivalent to angular restriction, as can be seen from the second term in Eq. 22. An increase of C by a factor 2 yields the same effect on V_{oc} (and therefore on η) as a decrease of ε_c by a factor 2. Since $C_{max}\,\varepsilon_s = \pi$, applying no concentration and maximum angular restriction ($\varepsilon_c = \varepsilon_s$) gives the same effect as applying maximum concentration and no angular restriction.

Furthermore, for each of these three cases, optimum bandgap values and maximum efficiencies are also obtained under the constraint that three of these bandgaps must be those of crystalline silicon (c-Si), amorphous silicon (a-Si) and germanium (Ge).

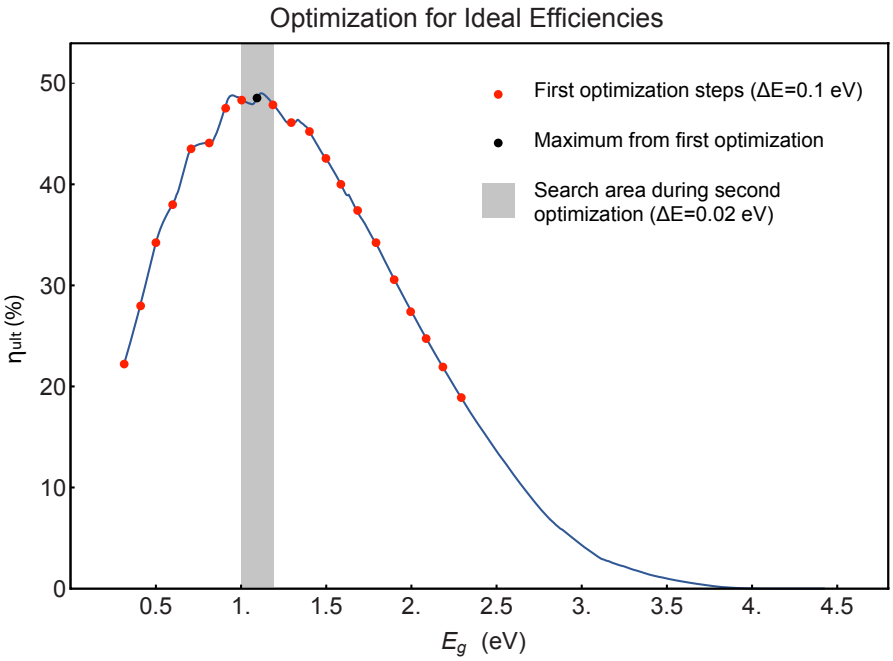

Figure 4: Example of the optimization procedure for finding an ideal efficiency limit, here for the case of the ultimate efficiency of a single junction cell. The first part of the optimization is a crude exploration of the parameter space in steps of 0.1 eV. The second part consists of a finer exploration (in steps of 0.02 eV) of that region of parameter space (grey band) that lies around the optimum value found during the crude exploration.

3.2 Material Requirements

In the second part of the work, where we obtain more realistic efficiencies for solar cells, a study was performed to find existing semiconductor materials having bandgaps close to the optimum values found for no concentration or angular restriction. The materials that we propose must obey the following criteria:

- They do not contain rare chemical elements.
- The elements that are contained must be obtainable in an economically feasible manner, that is they must exist in high concentrations in e.g. ore.
- They do not contain highly poisonous elements, such as Cd or Hg.
- The materials should have as high as possible absorption coefficients for photon energies above the bandgap. This is important firstly for fabrication of thin films and secondly because high absorption coefficients usually also indicate low radiative lifetimes, resulting in a higher quantum efficiency of radiative recombination.
- They are not known to contain high defect densities, which would result in high non-radiative recombination rates.

Using the bandgap energies of the materials thus found, we then study efficiencies of single junction and multi-junction cells depending on the parameters mentioned above: the number of junctions, concentration C, limiting output angle θ_{lim} and χ.

3.3 Uncertainty

Two effects cause an uncertainty in the values obtained for efficiencies: the finite resolution during the exploration of the bandgap parameter space and the ideal diode approximation.
The first uncertainty is due to the fact that when one explores parameter space with a certain resolution, there is always a chance that the maximum that is found is a local maximum and not the absolute maximum. Although the chance of this happening is small, since generally peaks were flat compared to the resolution of 0.1 eV, we estimated the maximum error to arise from this effect to be +0.8 % efficiency. This is based on observation of the sharpest peak in efficiency that we found for a 3-junction cell. Note that this is an error only in the positive direction, i.e. if our maximum efficiency is a local maximum, the absolute maximum efficiency can only be higher than this value. This uncertainty is only an issue in the first part of the simulations, where bandgaps were optimized to obtain ideal efficiency limits.
The second cause for uncertainty is the ideal diode approximation. Due to the assumption that was made (Eq. 14), the resulting expression for efficiency in Eq. 27 produces an inexact result for cases where V_{oc} is close to E_g. This is only the case for high ratios of short-circuit current to dark current, i.e. maximum concentration or, as long as $\chi = 1$, maximum angular restriction. As shown in appendix B, this error is $\sim 0.05\%$ efficiency for a single junction cell ($E_g = 1.12$eV) under maximum concentration. The error for a subcell in a multi-junction solar cell is expected to be less, as these absorb a smaller part of the solar spectrum and thus have lower light-generated current. Nevertheless, we take this 0.05 % efficiency as the deviation per subcell, and only for cells under maximum concentration. In the case of no concentration or the case of maximum angular restriction and $\chi \neq 1$, this origin of uncertainty is negligible.

4 Results

In the following section, we present the results of our study. The first part deals with the ideal efficiency limits that were found for cells with 1 to 8 junctions by optimizing bandgap values. Maximum values were found for the ultimate efficiency η_{ult}, the efficiency for maximum concentration and the efficiency for no concentration or angular restriction.
The second part consist of three sections and concerns more realistic calculations of efficiency. First, we present existing materials that match the ideal bandgap values and that satisfy the requirements that were set in chapter 3.2. Secondly, we use the bandgap values of these materials to study efficiencies of a single junction cell, as a function of C and θ_{lim} for different χ. Third, we study efficiencies of a multi-junction cell for different χ, both for maximum concentration and for maximum angular restriction.
In the last part of this chapter we study two particular cases of solar cell configuration more closely. We consider first the single junction c-Si cell, where we discuss the origin of the losses that occur and the improvements of its efficiency that are possible by using concentration or angular restriction. The same analysis is then carried out for a 5-junction Ge-(c-Si)-CZTS-(a-SiC)-GaP cell.

4.1 Ideal Efficiency Limits for 1-8 Junction Solar Cells

In this section, χ is set to unity and bandgaps were optimized to find maximum values for the ultimate efficiency η_{ult}, the efficiency for maximum concentration and the efficiency for no concentration or angular restriction. This was done for 1 to 8 junction solar cells, for both the case where all subcell bandgap energies were varied, as well as the case where three of the bandgaps were set to the bandgaps of germanium (0.67 eV), crystalline silicon (1.12 eV) and amorphous silicon (1.7 eV). Efficiencies obtained were also compared to literature. The results are shown in Fig. 5. The optimum bandgap values that were found are listed in appendix C.

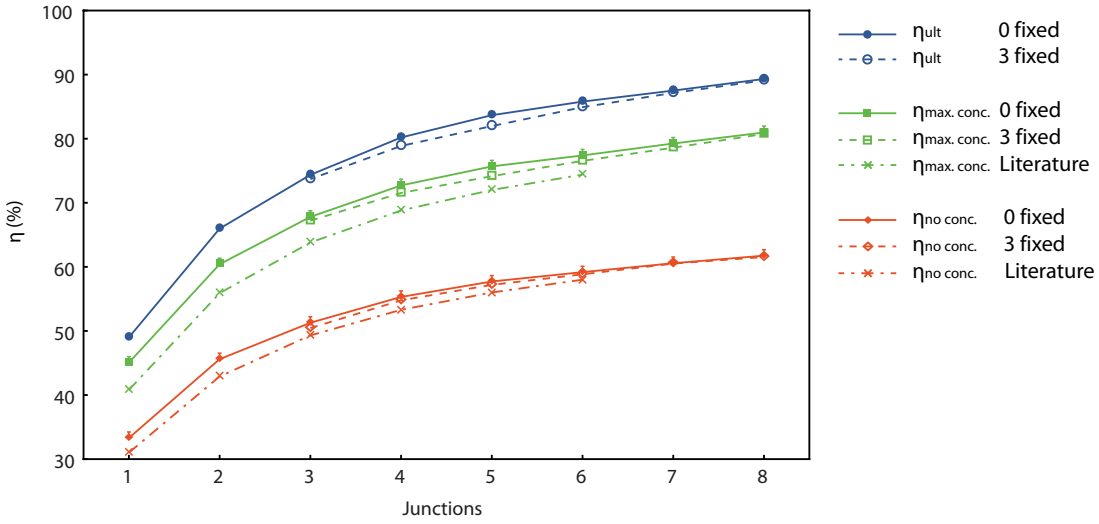

Figure 5: Maximum efficiencies for solar cells with 1 to 8 junctions, assuming $\chi = 1$. Ultimate efficiency (η_{ult}), efficiency for maximum concentration ($\eta_{max.\,conc.}$) and efficiency for no concentration or angular restriction ($\eta_{no\,conc.}$) are shown. Also, results are shown for the case where all bandgaps were varied (full lines) as well as the case where 3 bandgaps were set to the 0.67 eV, 1.12 eV and 1.7 eV (the bandgaps of Ge, c-Si and a-Si, respectively) and the other bandgaps were varied (dashed lines). The dot dashed lines represent values found in literature [7], where an ideal blackbody spectrum was used for the solar radiation.

Firstly, it can be seen in Fig. 5 that the efficiency increases continuously with the number of cell junctions, however the increase in efficiency per junction added becomes low after 4 or 5 junctions ($\sim 2\%$ efficiency per junction). This occurs for η_{ult} as well as the efficiencies for maximum and no concentration. It indicates that the origin of the increase of efficiency is the reduction of thermalization and non-absorption losses, which are the only losses present in all three types of efficiency. These losses are strongly reduced by the addition of a second or a third junction to the cell, which allows for a much larger part of the spectrum to be efficiently absorbed, whereas reduction of these losses saturates for addition of more than 4 or 5 junctions.

Secondly, setting 3 bandgap energies to those of Ge, c-Si and a-Si does not seem to have a dramatic effect on efficiency. Differences are usually of the order of 1 %. This can be interpreted in two ways: either the bandgaps of c-Si, a-Si and Ge are close to the optimum bandgap values that were found, or alternatively the maximum efficiency is not a very sharp maximum and there exist many combinations of bandgaps that reach almost the same efficiency. In any case, this is a positive result, as it allows for the use of these well-characterized semiconductors in the design of the solar cell.
Thirdly, the difference in efficiency between the blue and the green curves, which can be attributed to the blackbody radiation from the cells, grows with the number of junctions, from 3.4 % for a single junction cell to 8.4 % for a cell with eight junctions. This behavior can be understood by realizing that each subcell adds its own blackbody radiation to that of the total cell, since the area of one subcell is constant irregardless of the number of subcells. This means that for example an 8-junction cell has an area twice as large as a 4 junction cell, and therefore more blackbody radiative losses. This effect decreases the efficiency slightly for higher number of junctions, causing the growing difference between the blue and the green graph. Because of this, it is also expected that after a certain number of junctions (assuming that the area of a subcell remains constant, as we have done here), the efficiency will decrease, because the reduction of thermalization and non-absorption losses no longer compensates for the increased blackbody radiation.
Fourthly, it can be observed that the increase in efficiency due to concentration grows with the number of junctions, from 11.8 % for a single junction cell to 19.2 % for eight junctions. This is due to two effects: firstly the thermalization losses, which are the main constraint on efficiency for a single junction cell, are decreased for higher number of junctions, allowing for more improvement of efficiency by concentration. Secondly, concentration is most effective for cells with narrow bandgaps, which are present more in cells with high number of junctions. This is because the difference in V_{oc} between cells with maximum concentration and no concentration is, according to Eq. 22:

$$\frac{kT_c}{q}\ln\left(C_{max}\right) = 0.278V$$

This is a larger relative increase of V_{oc} for cells with lower bandgap, which may have a V_{oc} as low as 0.3 V (for $E_g \approx 0.5$ eV) under unconcentrated illumination. Therefore, for these subcells, concentration can cause roughly a doubling of output power.
Finally, maximum efficiencies lie above literature values. Differences are $\sim 4\%$ for maximum concentration and $\sim 2.5\%$ for no concentration. This difference is however expected, since for these literature values an ideal blackbody spectrum was taken for the solar irradiation, whereas we have used the AM1.5 D spectrum. This produces higher efficiencies, as one can reduce thermalization losses and non-absorption losses by tuning the bandgaps such that they match the peaks and dips in the spectrum, absorbing most efficiently in areas of the spectrum with high intensities. It is shown by Baruch et al. [4] that the difference in maximum efficiencies due to these different spectra, in the case of a single junction cell with no concentration, is $\sim 3\%$. This matches the difference we observe.

4.2 Realistic Efficiencies

In this section we present more realistic calculations of efficiency. First, we present existing materials that match the ideal bandgap values and that satisfy the requirements that were set in chapter 3.2. Then, in the second and the third part, we study efficiencies of respectively a single junction cell and multi-junction cells for different values of χ, C and θ_{lim}.

4.2.1 Real Solar Cell Materials

Here, we present existing materials that match the ideal bandgap values found for multi-junction solar cells with 1 to 8 junctions under no concentration. These values are listed in appendix C. The materials that we found satisfy the conditions that were listed in chapter 3.2.

A list of semiconductor materials containing only abundant and non-toxic elements with bandgap energies between 0.5 and 2.5 eV can be found in appendix D, showing the materials, their bandgaps, whether these bandgaps are direct or indirect, and literature on those materials. The materials that we propose to use for solar cells with 1 to 8 junctions are listed in Table 1. [6]

[6]Note that the material listed as $Cu_2ZnSn(S_xSe_{1-x})$ in this table is referred to in the rest of this work by its abbreviation CZTS.

Junc-tions	Fixed	G1 material	G1 (eV)	G2 material	G2 (eV)	G3 material	G3 (eV)	G4 material	G4 (eV)	G5 material	G5 (eV)	G6 material	G6 (eV)	G7 material	G7 (eV)	G8 material	G8 (eV)
1	0	c-Si	1.12	-	-	-	-	-	-	-	-	-	-	-	-	-	-
2	0	β-$FeSi_2$	0.86	a-Si	1.70	-	-	-	-	-	-	-	-	-	-	-	-
3	0	β-$FeSi_2$	0.86	$Cu_2ZnSn(S_xSe_{1-x})$	1.40	Cu_2O	2.00	-	-	-	-	-	-	-	-	-	-
3	3	Ge	0.67	c-Si	1.12	a-Si	1.70	-	-	-	-	-	-	-	-	-	-
4	0	Ge	0.67	c-Si	1.12	$Cu_2ZnSn(S_xS_{1-x})$	1.57	ZnP_2	2.10	-	-	-	-	-	-	-	-
4	3	Ge	0.67	c-Si	1.12	a-Si	1.70	GaP	2.26	-	-	-	-	-	-	-	-
5	0	Ge	0.67	c-Si	1.12	$Cu_2ZnSn(S_xSe_{1-x})$	1.40	a-SiC	1.80	GaP	2.26	-	-	-	-	-	-
5	3	Ge	0.67	c-Si	1.12	$Cu_2ZnSn(S_xSe_{1-x})$	1.40	a-Si	1.70	GaP	2.26	-	-	-	-	-	-
6	0	$CuFeS_2$	0.53	β-$FeSi_2$	0.86	c-Si	1.12	a-SiGe:H	1.50	Cu2O	1.90	3C-SiC	2.40	-	-	-	-
6	3	Ge	0.67	β-$FeSi_2$	0.86	c-Si	1.12	$Cu_2ZnSn(S_xSe_{1-x})$	1.40	a-Si	1.70	GaP	2.26	-	-	-	-
7	0	$CuFeS_2$	0.53	β-$FeSi_2$	0.86	c-Si	1.12	$Cu_2ZnSn(S_xSe_{1-x})$	1.40	a-Si	1.70	ZnP_2	2.10	$CuAlS_2$	2.50	-	-
7	3	Ge	0.67	β-$FeSi_2$	0.86	c-Si	1.12	$Cu_2ZnSn(S_xSe_{1-x})$	1.40	a-Si	1.70	ZnP_2	2.10	$CuAlS_2$	2.50	-	-
8	0	$CuFeS_2$	0.53	Ge	0.67	β-$FeSi_2$	0.86	c-Si	1.12	$Cu_2ZnSn(S_xSe_{1-x})$	1.40	a-Si	1.70	ZnP_2	2.10	$CuAlS_2$	2.50
8	3	$CuFeS_2$	0.53	Ge	0.67	β-$FeSi_2$	0.86	c-Si	1.12	$Cu_2ZnSn(S_xSe_{1-x})$	1.40	a-Si	1.70	Cu_2O	2.00	$CuAlS_2$	2.50

Table 1: Multi-junction solar cells consisting of semiconductor materials with bandgaps close to the ideal bandgap values. G1 denotes the subcell with the lowest bandgap energy, G2 the subcell with the next lowest bandgap energy etc. Materials are listed, as well as their reported bandgap values. The column 'Fixed' indicates the number of bandgaps that were fixed during the optimization of bandgaps, as is mentioned in chapter 4.1.

4.2.2 The Single Junction Cell

Here we calculate the efficiencies of a single junction cell as a function of concentration C and limiting output angle θ_{lim} for different values of χ. The bandgap of the cell is that of c-Si (1.12 eV), the material that was suggested in the previous section for a single junction cell. Results for efficiency as a function of C and θ_{lim} are shown in Fig. 6 and 7 respectively.

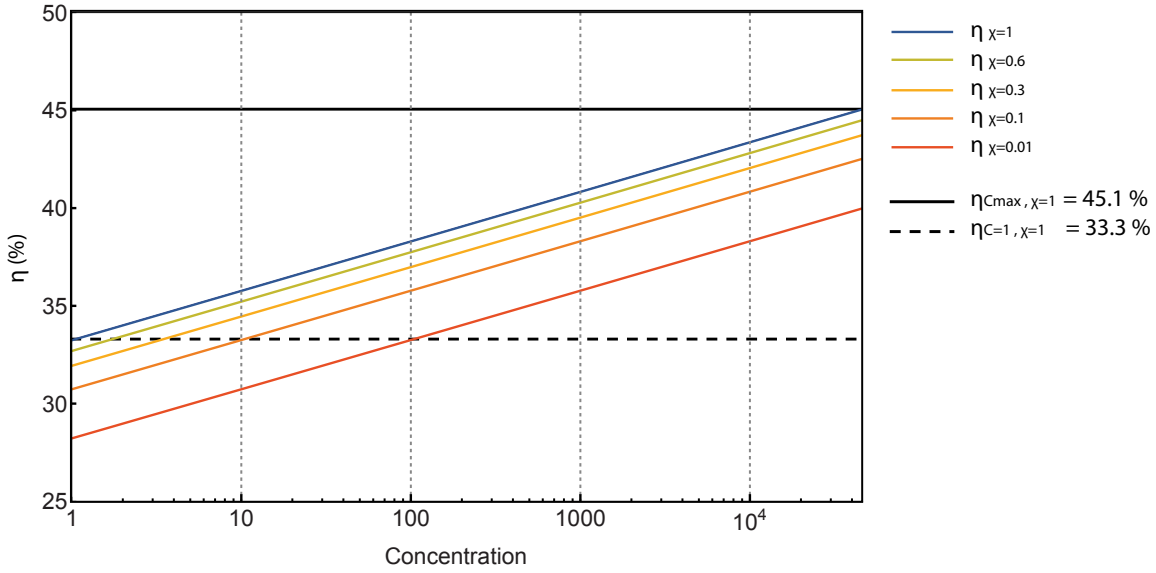

Figure 6: Efficiency of a single junction c-Si cell as a function of concentration (C), where C ranges from 1 to C_{max} ($\sim$ 46000). Plots for different values of χ are shown in colors. The thick black line and the thick, dashed black line indicate the optimal efficiency of a single junction cell with $\chi = 1$, under maximum concentration (45.1%) and no concentration or angular restriction (33.3%), respectively. Vertical dashed lines indicate concentration levels of 10, 100, 1000 and 10000 suns.

In Fig. 6 we can observe two trends: Firstly, the overal efficiency of the cell decreases with lower χ. This is because lowering χ means increasing non-radiative recombination rate and therefore dark current. Secondly, the effect of increased concentration is the same for any value of χ. That is, efficiency depends logarithmically on C and although lowering χ may decrease the overall efficiency, it does not influence this dependency on C. Both these trends can be explained by considering the expression for V_{oc} (Eq. 22). Taking $\varepsilon_c = \pi$, this equation shows that V_{oc} depends on χ and C in a logarithmic manner:

$$V_{oc} = ... + \frac{kT_c}{q}\left(\ln\left(\frac{C\varepsilon_s}{\pi}\right) + \ln(\chi)\right) \tag{33}$$

Moreover, the effects of χ and C are independent of each other. This is exactly what we observe in Fig. 6. It should be noted though, that this independency is due to our choice of definition of χ, and that in reality the ratio of radiative recombination and total recombination is not likely to be independent of concentration. By choosing χ to be independent of the voltage, we have assumed that the non-radiative recombination rate depends on voltage through the same factor $e^{\frac{qV}{kT}}$ as the radiative recombination rate. However, in reality Auger recombination depend much more strongly on voltage (through a factor $e^{\frac{3qV}{kT}}$) due to the strong dependency on carrier density [5, 10], and defect recombination usually depends less strongly on voltage (through a factor $e^{\frac{qV}{2kT}}$ for recombination in inter-band defect states [5]). χ therefore depends on cell voltage and since the cells operating voltage grows with the concentration factor C, χ also depends on C. Depending on whether Auger or defect recombination is the dominant source of non-radiative recombination, χ decreases or grows with C and the graphs in Fig. 6 for more realistic calculations should become less or more steep, respectively.

The decoupling of the effects of concentration and χ on efficiency observed in Fig. 6 is not found in the case of angular restriction though. As one can observe in Fig. 7, the effect of reducing θ_{lim} on the cell efficiency

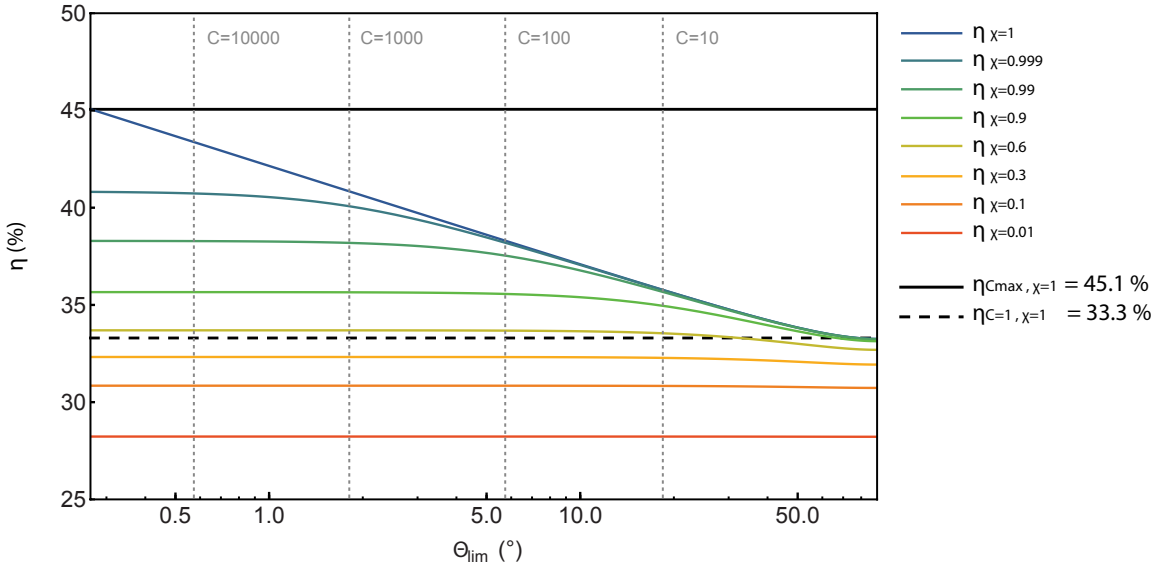

Figure 7: Efficiency of a single junction c-Si cell as a function of limiting output angle (θ_{lim}). Note that the figure is mirrored with respect to Fig. 6, i.e. decreasing θ_{lim} produces a similar effect on efficiency as increasing C. Plots for different values of χ are shown. The thick black line and the thick, dashed black line indicate the optimal efficiency of a single junction cell with $\chi = 1$, under maximum concentration (45.1%) and no concentration or angular restriction (33.3%), respectively. Vertical dashed lines indicate values for θ_{lim} that would produce the same effect on efficiency as concentration levels of 10, 100, 1000 and 10000 suns in a cell with unity χ. For cells with non-unity χ, this equivalence no longer holds.

depends very strongly on χ. For $\chi = 1$ angular restriction produces the same effect on efficiency as concentration, yielding a maximum improvement of efficiency of 11.8 %. However, for $\chi = 0.9$ the maximum gain in efficiency that is possible with angular restriction is already reduced to $\sim 2\%$. This is because lowering θ_{lim} decreases the radiative recombination rate, but does not influence the non-radiative recombination rate. Further reduction of θ_{lim} beyond the point where non-radiative recombination rate has become the dominant source of recombination therefore does not increase efficiency further. This explains why the curves with $0.6 \leq \chi \leq 1$ in Fig. 7 initially show an increase of efficiency as θ_{lim} is reduced below 90° and radiative recombination rate is still the dominant recombination source, but stabilize at a certain point when non-radiative recombination rate has become dominant.

These results imply that, whereas concentration remains a useful method of increasing solar cell efficiencies, irregardless of the level of non-radiative recombination, angular restriction is useful only for materials with very low non-radiative recombination rates ($\chi \geq 0.9$). The effect of concentration is however not expected to be independent of the dominant type of non-radiative recombination.

4.2.3 The Multiple Junction Cell

In this section, we generalize the studies from the previous section on single junction cells to the case of multi-junction cells. We study efficiencies of cells with 1 to 8 junctions for different χ, both for maximum concentration and for maximum angular restriction. Results for the former and for the latter case are shown in Fig. 8 and 9 respectively.

From Fig. 8, the following conclusions can be drawn: firstly, the use of real, existing materials does not lower efficiency much compared to use of the ideal bandgap values, as can be seen by the difference between the black and the blue curve. The largest difference between these two is ~ 3 % for a 3-junction cell. Secondly, it can be seen that, just as for the single junction cell, the efficiency for cells with any number of junctions under maximum concentration is lowered as χ decreases. This can be understood because the relation between the open circuit voltages of the subcells and χ is given by the same logarithmic term as for a single-junction cell (Eq. 33).

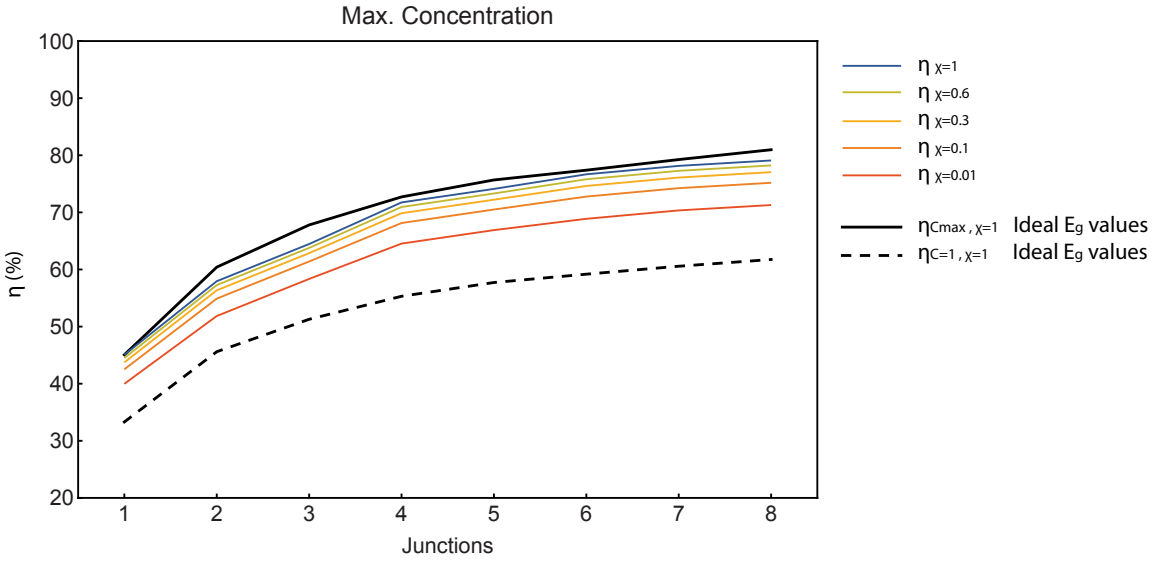

Figure 8: Efficiencies for solar cells with 1 to 8 junctions under maximum concentration, for several values of χ. The thick black line and the thick, dashed black line indicate the optimal efficiencies of the cells with $\chi = 1$, respectively under maximum concentration and no concentration or angular restriction. These correspond to the green and the orange full lines in Fig. 5.

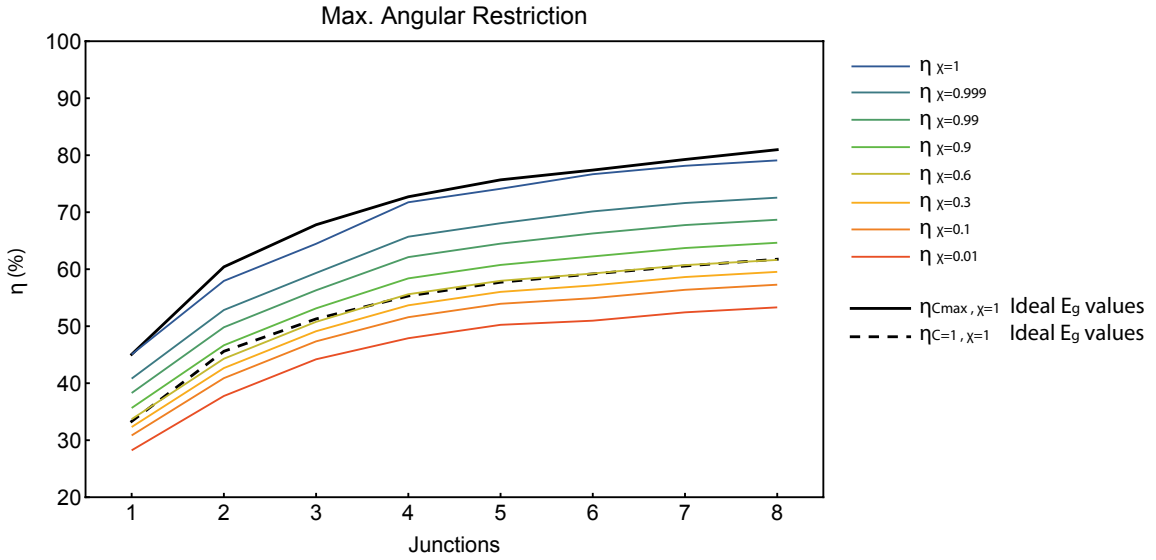

Figure 9: Efficiencies for solar cells with 1 to 8 junctions under maximum angular restriction, for several values of χ. The thick black line and the thick, dashed black line indicate the optimal efficiencies of the cells with $\chi = 1$, respectively under maximum concentration and no concentration or angular restriction. These correspond to the green and the orange full lines in Fig. 5.

In Fig. 9 we recognize the same strong dependency on χ of the effect of angular restriction on efficiency as we observed for the single junction cell. Efficiencies decrease drastically with χ, because non-radiative recombination has become the dominant source of recombination for non-unity χ and maximum angular restriction. Already for $\chi = 0.6$, we see that efficiencies are comparable to those for no concentration or angular restriction and $\chi = 1$ (the black, dashed line). The decrease of efficiency between the curves with $\chi = 1$ and $\chi = 0.999$ is slightly larger for higher number of junctions (due to the narrow bandgap subcells in these many-junction cells, as was mentioned in section 4.1), but in all other cases the decrease is the same for all number of junctions.

From these figures, it is clear that the effect we have seen in the previous section for single junction cells, holds for multi-junction cells as well. That is, whereas concentration remains useful as a means to increase efficiency regardless of what value χ has, angular restriction only produces a significant increase of efficiency for near-unity χ.

4.3 The single junction c-Si cell and the 5-junction Ge-(c-Si)-CZTS-(a-SiC)-GaP cell

In this section, we highlight the origin of losses and the potential for improvement of efficiencies in two specific cases: a single junction c-Si cell and a 5 junction Ge-(c-Si)-CZTS-(a-SiC)-GaP cell. This is because a single junction cell remains interesting for practical use, because of its simplicity relative to a multi-junction cell. Amongst the multi-junction cells, a 5-junction cell can be argued to have the maximum amount of subcells, after which addition of extra subcells would result in such a minor increases of efficiency that it would not be worth the effort. One could however also reasonably place this maximum at the 3 or 4-junction cell.

We shall take χ to be 0.1 in these cells, i.e. 90% of their recombination is non-radiative, which is an optimistic value for c-Si [15]. For most materials, χ will most likely be lower.
Losses in the cell are divided into:

- Thermalization and non-absorption losses. These losses are accounted for in the ultimate efficiency η_{ult}.
- Fundamental losses due to blackbody radiation. These losses lower efficiency from η_{ult} to the efficiency under maximum concentration and $\chi = 1$.
- Non-radiative recombination losses. These losses occur upon lowering χ from 1 to 0.1.
- Losses due to lack of concentration. These losses account for the difference between the efficiency of a cell with concentration C_{max} and a cell with $C = 1$.

Fig. 10 shows these losses and the resulting efficiency limits for both cells under consideration.

Considering Fig. 10, we can now compare the different loss terms between the single junction and the multi-junction cell.
The first loss term, thermalization and non-absorption, which is by far the largest loss term for a single junction cell, has been significantly reduced in the 5-junction cell. This is because the spectrum can be far more effectively absorbed by a multi-junction cell and thermalization losses are reduced because each subcell absorbs a smaller part of the spectrum, containing no photons that have energies far exceeding their bandgaps.
The second loss term, fundamental blackbody radiation losses, is larger in the multi-junction cell. This is due to the increased blackbody radiation upon addition of a subcell, as was explained in section 4.1.
The third term, non-radiative recombination losses, is also slightly higher for the 5-junction cell. This is because decreasing χ from 1 to 0.1 while keeping θ_{lim} constant at π causes a fixed decrease of V_{oc} given by $\frac{kT_c}{q} \ln\left(\frac{1}{0.1}\right) = 0.06V$ (see Eq. 22). As was the case for concentration, this leads to a higher relative decrease of V_{oc} in subcells with narrow bandgaps, which are found more in cells with high number of junctions. Therefore these cells are more sensitive to a decrease in χ.
As for the fourth loss term, losses due to lack of concentration, we see that these losses are again higher for the 5-junction solar cell. As explained in section 4.1, this is due to the presence of narrow-bandgap subcells in the multi-junction cell, which have higher relative gain of V_{oc} due to concentration.

It is clear that for both cells, concentration of solar light has the potential to make a large difference in solar cell efficiency: 11.6% and 16.7 % gain in efficiency under maximum concentration for the single junction and the 5-junction cell, respectively. Even though maximum concentration is impossible in practice, a concentration factor of e.g. 1000 would still give an increase in efficiency of 7.6 % for the single junction cell and 10.7% for the 5-junction cell.
The potential for efficiency gain due to angular restriction however, was not shown in Fig. 10, as it would have been to small to observe for $\chi = 0.1$. On the other hand, the difference between concentration and angular restriction for solar cell efficiency can clearly be seen in Fig. 11, where the energy produced by the 5-junction solar cell per nm wavelength is shown. Per subcell, the number of irradiated photons at each wavelength is

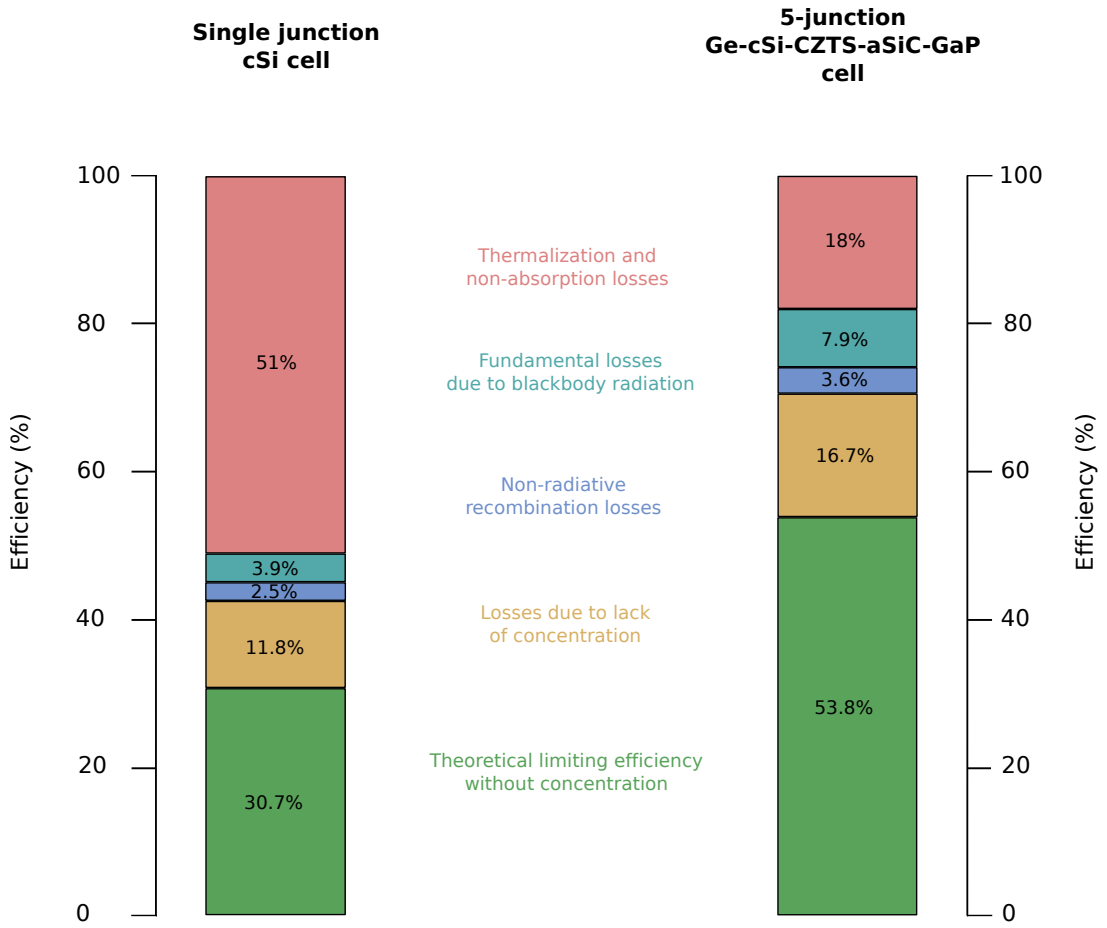

Figure 10: The losses and efficiency gain potential in a single junction c-Si cell and a 5-junction Ge-(c-Si)-CZTS-(a-SiC)-GaP cell. Both cells are assumed to have $\chi = 0.1$. The efficiency gain that is obtainable with angular restriction ($\sim 0.1\%$)is not shown.

multiplied by the subcells fill factor FF and q times open circuit voltage V_{oc} to obtain the produced power per wavelength. The area under each of these curves, divided over that under the solar spectrum, represents the efficiency of the solar cell with that particular configuration.

The blue curve represents energy production in a cell with ultimate efficiency. It overlaps with the solar spectrum at wavelengths corresponding to subcell bandgap energies, since these photons create carriers that do not thermalize. Furthermore, photons with energies below the bandgap of Ge are not absorbed. This would require a subcell with very low bandgap, which has near-zero V_{oc} for unconcentrated sunlight. These bandgap values are based on optimum values for unconcentrated sunlight (see appendix C.3).
The curves labeled "C_{max}, $\chi = 1$" and "$C = 1$, no ang. restriction, $\chi = 1$" represent the energy production in a cell with no non-radiative recombination and with respectively maximum concentration and no concentration or angular restriction. The curves labeled "C_{max}, $\chi = 0.1$" and "$C = 1$, max ang. restriction, $\chi = 0.1$" represent the energy production in a cell with 90% non-radiative recombination and with respectively maximum concentration and maximum angular restriction. Comparing these last two curves, it can be clearly seen that angular restriction produces much lower efficiency then concentration.

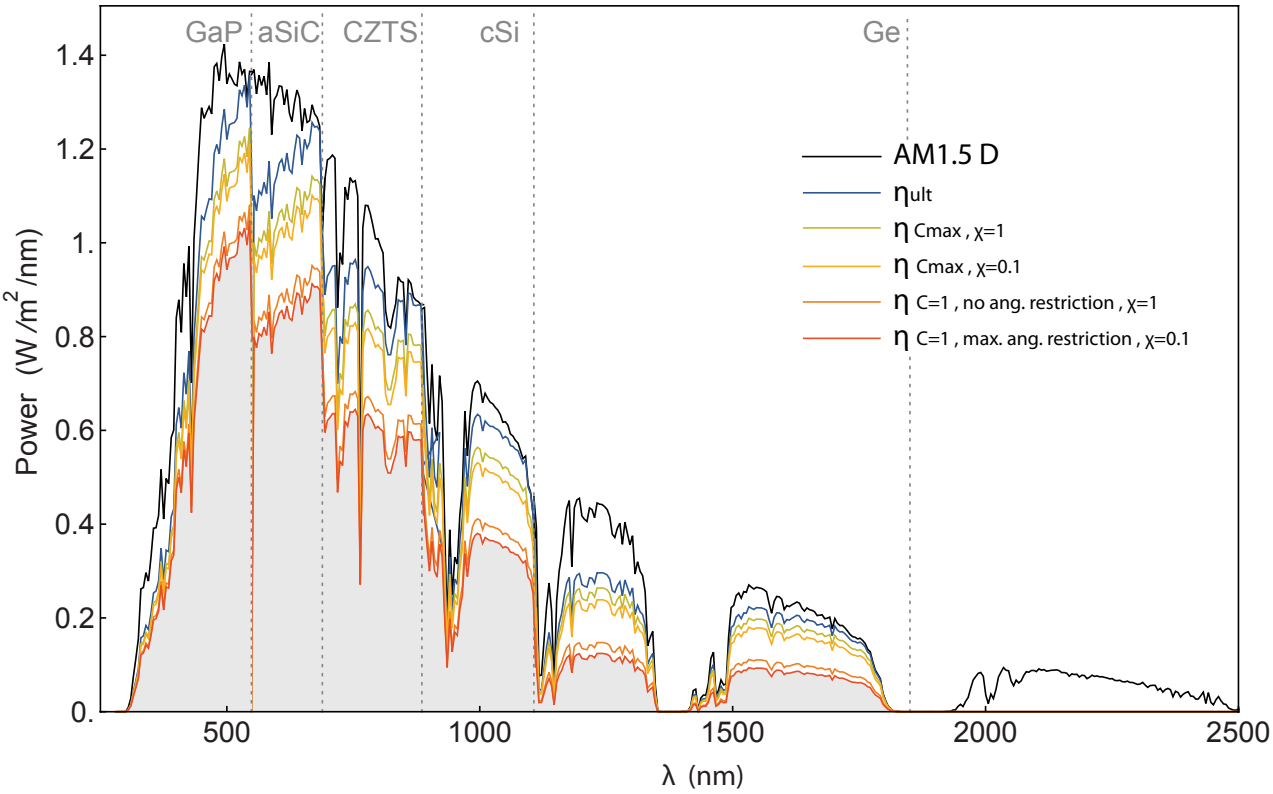

Figure 11: The energy produced per wavelength by the 5-junction Ge-(c-Si)-CZTS-(a-SiC)-GaP solar cell under different circumstances (colored curves), compared with the AM1.5 D solar spectrum (black curve). Efficiency of the cell in one of these circumstances is the area under the corresponding graph, divided by the area under the AM1.5 D solar spectrum. Vertical dashed lines indicate the wavelengths corresponding to the bandgaps of the subcell materials. For $\chi = 0.1$, angular restriction is less effective than concentration in increasing efficiency.

5 Discussion

These simulations give deep insight in the loss mechanisms and potential efficiencies of a solar cell through the systematical variation of the number of junctions, concentration, angular restriction and non-radiative recombination rate.
Optimum efficiency values that were found for cells with 1 to 8 junctions vary slightly from literature values, which can however be contributed to use of a different solar spectrum. The dependency of efficiency on angular restriction for a single junction solar cell that was observed in section 4.2.2 resembles the results found by Kosten et al. [10] for a single junction GaAs cell with several values for internal fluorescent yield (a quantity comparable to the parameter χ). Our suggestion that angular restriction is only useful in cells with less than 10% non-radiative recombination (i.e. $\chi \geq 0.9$), is affirmed by the work of Martí et al. [11].

To further improve the simulations, the following suggestions could be considered.
Firstly, simulations should be expanded so as to account for imperfect light trapping. In this work, perfect light absorption was assumed. Taking into account realistic light trapping scenarios with absorption depending on absorption coefficient, cell thickness and surface texturing (as Kosten et al. have done for GaAs cells [10]) would lead to more accurate efficiencies.
Secondly, in stead of the macroscopic parameter χ, a more detailed description of non-radiative recombination losses can be incorporated in the simulations. Empirical descriptions based on material parameters exist for the recombination rates due to Auger recombination [10] as well as surface defect and bulk defect recombination [5]. This adjustment would require knowledge of material parameters such as absorption coefficient and carrier densities, lifetimes and mobilities. It would complicate simulations, especially because it would no

longer be possible to use the Shockley-Queisser model due to the different dependencies of the recombination rates on cell voltage. The exact model could be used instead, and one could study e.g. the performance of the suggested solar cell material combinations (Section 4.2.1).
Thirdly, non-unity transmittance of solar illumination can be taken into account by incorporating into the model for example single-layer or multi-layer antireflection coatings that are optimized for the spectral range of a specific subcell.

A good step towards reaching a highly efficient, low-cost solar cell would be to focus on the two designs proposed in section 4.3.
The single junction c-Si cell remains the best characterized and most developed solar cell today, and it is worth looking into improving its efficiency in such a way that it can be easily incorporated in the existing production process. Its efficiency could be improved by 7.6 % employing 1000-fold concentration of the light.
For higher efficiencies, one could focus on the 5 junction Ge-(c-Si)-CZTS-(a-SiC)-GaP cell suggested here. Using a spectrum splitter and a concentrator, this cell, consisting of only abundant materials for which χ is assumed to be 0.1, could reach efficiencies of 64.5% for 1000-fold concentration.

6 Conclusion

We have used the detailed balance model to calculate theoretical efficiencies of solar cells. The number of subcells, solar concentration, limiting output angle and non-radiative recombination rate were varied and their influence on efficiency was studied. Existing and abundant materials were proposed for use in multi-junction solar cells.
From ideal efficiency calculations, it is found that for cells with more than 5 junctions, efficiency increase per junction added is max. $\sim 2\%$, making it superfluous to use more than 5 subcells in a multi-junction cell. Next, more realistic efficiency calculations were performed including non-radiative losses, where it was observed that concentration is a useful means to increase efficiency of the solar cell for any non-radiative recombination rate. The effect of restricting the angle of emitted light, on the other hand, becomes almost negligible ($\leq 2\%$ increase in efficiency) as χ drops below 0.9, that is for more than 10 % of the recombination being non-radiative. Finally, an analysis of the single junction c-Si cell and the 5-junction Ge-(c-Si)-CZTS-(a-SiC)-GaP cell reveals that, assuming $\chi = 0.1$, the former has a potential efficiency of 30.7 % for unconcentrated light and 38.3 % for a concentration of 1000 suns, and the latter has potentially 53.8 % efficiency for unconcentrated light and 64.5 % for a concentration of 1000 suns.
This study has provided detailed insight into the relative contributions of loss processes in solar cells, which were summarized by comparing the losses in a single junction and a 5-junction cell, as well as made suggestions for the fabrication of very high efficiency solar cells. These results may serve as guidelines in the continued search for a highly efficient solar energy system fit for large-scale applications.

7 Acknowledgments

Ik wil mijn begeleider Jorik van de Groep en Albert Polman hartelijk danken voor de uitstekende begeleiding. Jullie gedetailleerde en accurate commentaar op mijn werk, evenals jullie hulpvaardigheid en de inspirerende gesprekken die we hebben gevoerd, hebben ervoor gezorgd dat ik in de korte tijd die ik bij jullie in de groep heb doorgebracht meer heb kunnen leren dan ik voor mogelijk had gehouden.

I would also like to thank the entire Photonic Materials Group at AMOLF for the wonderful cooperation and the much-appreciated comic relief.

References

[1] P.T. Landsberg and G. Tonge
Thermodynamic energy conversion efficiencies, *J. Appl. Phys.* 51, R1 (1980)

[2] A. Martí and G.L. Araújo
Limiting efficiencies for photovoltaic energy conversion in multigap systems, *Sol. En. Mat. Sol. Cells* 43, 203-222 (1996)

[3] T. Markvart
Thermodynamics of losses in photovoltaic conversion, *Appl. Phys. Lett.* 91, 064102 (2007)

[4] P. Baruch, A. De Vos, P.T. Landsberg and J.E. Parrott
On some thermodynamic aspects of photovoltaic solar energy conversion, *Sol. En. Mat. Sol. Cells* 36, 201-222 (1995)

[5] A. Luque and S. Hegedus
Handbook of Photovoltaic Science and Engineering, Wiley (2011)

[6] W. Shockley and H.J. Queisser
Detailed balance limit of efficiency of p-n junction solar cells, *J. Appl. Phys.* 32, 510-519 (1961)

[7] M.A. Green
Third Generation Photovoltaics, Springer (2003)

[8] A.S. Brown and M.A. Green
Limiting Efficiency for Current-Constrained Two-Terminal Tandem Cell Stacks, *Prog. Photovolt: Res. Appl.* 10, 299-307 (2002)

[9] A. de Vos
Detailed balance limit of the efficiency of tandem solar cells, *J. Phys. D: Appl. Phys.* 13, 839-846 (1980)

[10] E.D. Kosten and H.A. Atwater
Limiting acceptance angle to maximize efficiency in solar cells, *Proceedings of SPIE* 8124 (2011); doi:10.1117/12.894226

[11] A. Martí, J.L. Balenzategui and R.F. Reyna
Photon recycling and Shockley's diode equation, *J. Appl. Phys.* 82, 4067 (1997)

[12] G. Smestad and H. Ries
Luminescence and current-voltage characteristics of solar cells and optoelectronic devices, *Sol. En. Mat. Sol. Cells* 25, 51-71 (1992)

[13] P. Spinelli, M.A. Verschuuren and A. Polman
Broadband omnidirectional antireflection coating based on subwavelength surface mie resonators, *Nature Communications* 3, 692 (2012)

[14] H.A. Atwater and A. Polman
Plasmonics for improved photonic devices, *Nature Materials* 9, 174-177 (2010)

[15] A. Polman and H.A. Atwater
Photonic design principles for ultrahigh-efficiency photovoltaics, *Nature Materials* 11, 205-213 (2012)

[16] A. Barnett et al.
Milestones towards 50% efficient solar cell modules, *Proc. 22nd European Photovoltaic Solar Energy Conference* (2007)

[17] M.A. Green and A. Ho-Baillie
Forty three per cent composite split-spectrum concentrator solar cell efficiency, *Prog. Photovolt: Res. Appl.* 18, 42-47 (2010).

[18] Wikipedia, Étendue
http://en.wikipedia.org/wiki/Etendue (July 1st, 2012)

[19] D.L. Lide
Handbook of Chemistry and Physics, 88th ed., CRC press, 2008.

[20] C.C. Uhuegbu
Growth and Characterization of Lead Sulphide Thin Film for Solar Cell Fabrication, *Can. J. Scientific and Industrial Res.* 2, 230-241 (2011)

[21] L. Barkat et al.
Growth and characterization of CuFeS2 thin films, *J. Crystal Growth* 297, 426-431 (2006).

[22] D.J. Friedman and J.M. Olson
Analysis of Ge junctions for GaInP/GaAs/Ge three-junction solar cells, *Prog. Photovolt: Res. Appl.* 9, 179-189 (2001)

[23] B.A. Andersson
Materials availability for large-scale thin-film photovoltaics , *Prog. Photovolt: Res. Appl.* 9, 179-189 (2001)

[24] R. Braunstein et al.
Intrinsic Optical Absorption in Germanium-Silicon Alloys, *Physical Review*, 109, 3, 695-710 (1958).

[25] A. Vantomme et al.
Growth mechanism and optical properties of semiconducting Mg2Si thin films, *Microelectronic Engineering* 50, 237242 (2000)

[26] C. Wadia, A.P. Alivisatos and D.M. Kammen
Materials Availability Expands the Opportunity for Large-Scale Photovoltaics Deployment, *Environ. Sci. Technol.* 43, 2072-2077 (2009)

[27] Y. Makita
Materials availability for thin film solar cells, *AIP conf. proc.* 404, 3 (1997)

[28] Y. Makita et al.
A thin-film solar cell of high-quality b-FeSi2/Si heterojunction prepared by sputtering, *Sol. En. Mat. Sol. Cells* 90, 276-282 (2006).

[29] P.K. Nair et al.
Semiconductor thin films by chemical bath deposition for solar energy related applications, *Sol. En. Mat. Sol. Cells* 52, 313-344 (1998).

[30] K. Ellmer and H. Tributsch
Iron disulfide (pyrite) as photovoltaic material: problems and opportunities, *Proc. 12th Workshop on Quantum Solar Energy Conversion (QUANTSOL)*, 2000

[31] E. Mellikov et al.
Monograin materials for solar cells, *Sol. En. Mat. Sol. Cells* 93, 65-68 (2009).

[32] T. K. Todorov, K. B. Reuter and D. B. Mitzi
High-Efficiency Solar Cell with Earth-Abundant Liquid-Processed Absorber, *Adv. En. Mater.* 22, E156-E159 (2010)

[33] M.A. Green
Solar Cells, Un. of New South Wales (1992)

[34] Q. Xu et al.
Crystal and electronic structures of Cu_x]S solar cell absorbers, *Appl. Phys. Lett.* 100, 061906 (2012)

[35] A. Ogwu et al.
Electrical resistivity of copper oxide thin films prepared by reactive magnetron sputtering, *J. Achievements in Materials and Manufacturing Engineering* 24, 172-177 (2007)

[36] Y.S. Lee et al.
Earth abundant materials for high efficiency heterojunction thin film solar cells, *Photovoltaic Specialists Conference (PVSC)* (2009)

[37] B.P. Nelson et al.
Narrow gap a-SiGe:H grown by hot-wire chemical vapor deposition, *Thin Solid Films* 430, 104-109 (2003)

[38] Y. Xu et al.
Improving narrow bandgap a-SiGe:H alloys grown by hot-wire chemical vapor deposition, *Thin Solid Films* 430, 197-201 (2003)

[39] J. Yang, A. Banerjee and S. Guha
Triple junction amorphous silicon alloy solar cell with 14.6% initial and 13 % stable conversion efficiencies, *Appl. Phys. Lett.* 70, 2975 (1997)

[40] D.L. Staebler and C.R. Wronski
Reversible conductivity changes in dischargeproduced amorphous Si, *Appl. Phys. Lett.* 31, 292 (1977)

[41] X. Lu
Design, Fabrication, Characterization and Analysis of wide band gap GaP cells (PhD thesis), Un. of Delaware (2011)

[42] C.R. Allen, J. Jeon, J.M. Woodall
Simulation assisted design of a gallium phosphide n-p photovoltaic junction, *Sol. En. Mat. Sol. Cells* 94, 865-868 (2010)

[43] G.L. Harris
Properties of Silicon Carbide, INSPEC (1995).

[44] T. Chassagne et al.
A comprehensive study of SiC growth processes in a VPE reactor, *Thin Solid Films* 402, 83-89 (2002)

[45] H. Nagasawa, K. Yagi and T. Kawahara
3C-SiC hetero-epitaxial growth on undulant Si(0 0 1) substrate, *J. Crystal Growth* 237-239, 1244-1249 (2002)

[46] T.J. Alwan and M.A. Jabbar
Structure and optical properties of CuAlS2 thin films prepared via chemical bath deposition, *Turk. J. Phys.* 34, 107-116 (2010)

Appendices

A Étendue

Consider the situation in Fig. 12a, where an infinitesimal surface element dS is embedded in a medium with refractive index n. The surface emits light confined to a certain solid angle element $d\Omega$ at an angle θ with its normal vector $\mathbf{n}_S$. The area of dS that is projected in the propagation direction of the light is $dScos(\theta)$. The element of étendue of this light is then defined as [3] [18]:

$$d\varepsilon = n^2 cos(\theta) d\Omega dS \tag{34}$$

Note that since solid angle and n are dimensionless quantities, the dimension of étendue is area.

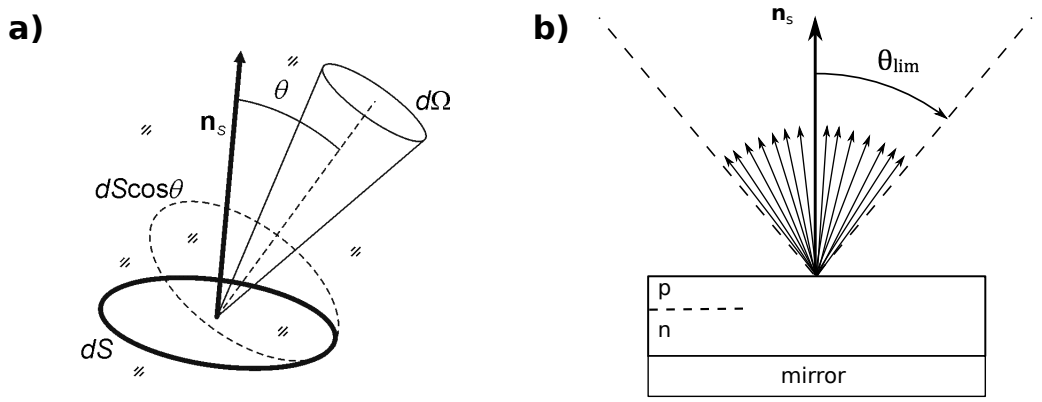

Figure 12: a) An infinitesimal surface area dS emitting light into an element of solid angle $d\Omega$ [18]. **b)** A planar solar cell with a mirror at the back with its outgoing cone of radiation extending to an angle θ_{lim}.

Fig. 12b depicts the case of a planar solar cell with a back reflector that is emitting radiation confined to a cone centered on the normal vector to the cells surface and extending to an angle θ_{lim}. The étendue of this radiation is given as:

$$\varepsilon = n^2 \int\int cos(\theta)\, d\Omega dS \quad = 2\pi\, n^2 A \int_0^{\theta_{lim}} cos(\theta)\, d\theta \quad = \pi\, n^2 A\, sin^2(\theta_{lim}) \tag{35}$$

A denotes the area of the solar cell. In this work, we are interested in the étendue per unit area of a solar cell that emits light constrained by various angles θ_{lim} into air (n=1). This étendue is hence given as:

$$\varepsilon = \pi\, sin^2(\theta_{lim}) \tag{36}$$

Note that for incoming radiation, étendue is defined in the same way, with $d\Omega$ now the solid angle subtended by the source of radiation, from the perspective of the receiver.

B Validity of the Ideal Diode Equation

As has been discussed in section 2.3, the ideal diode equation (Eq. 17) is an approximation of the exact current-voltage characteristic, valid for $E_g - qV_{oc} \gg kT_c$. However in some cases considered in this work, i.e. for $C = C_{max}$ or for maximum angular restriction and $\chi = 1$, this condition is no longer fulfilled. Eq. 21 then no longer describes open circuit voltage correctly and may even give V_{oc} higher than $\frac{E_g}{q}$. However, this leads only to a minor inaccuracy in the efficiency that is obtained, because the maximum power point hardly differs from the exact result. This is demonstrated in Fig. 13, taken from the work of Baruch et al. [4]. The authors show exact and approximate current-voltage and efficiency-voltage relations for a single junction cell with a bandgap of 1.1 eV, under maximum concentration and with only radiative losses. A perfect blackbody spectrum at a temperature of 5800 K was used for the solar irradiation. qV_{oc} exceeds E_g for the approximate solution, which yields a maximum efficiency for the exact and for the approximate case of 40.668% and 40.611% respectively, showing a difference of ∼0.05% efficiency.

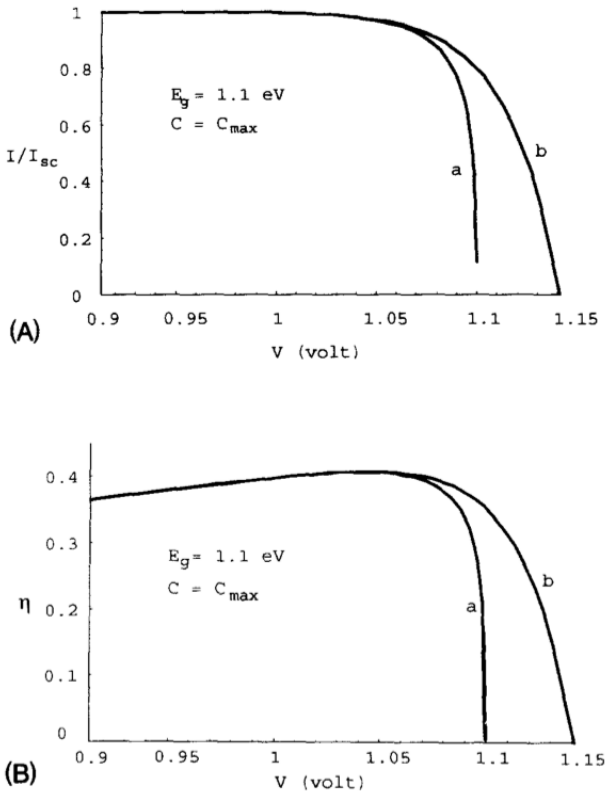

Figure 13: Current **(A)** and efficiency **(B)** plotted as a function of cell voltage, for a single junction cell with a bandgap of 1.1 eV, under maximum concentration and with only radiative losses. Curve **a** was calculated using the exact detailed balance model, curve **b** using the ideal diode equation (Eq. 17). This figure was taken from the work of Baruch et al. [4]

C Optimum Efficiencies and Bandgap Energies

C.1 Ultimate Efficiency

Junctions	Fixed	G1	G2	G3	G4	G5	G6	G7	G8	η_{ult} (%)
1	0	1.12	-	-	-	-	-	-	-	49.0
2	0	0.70	1.46	-	-	-	-	-	-	66.0
3	0	0.53	1.13	1.81	-	-	-	-	-	74.4
3	3	0.67	1.12	1.70	-	-	-	-	-	73.7
4	0	0.51	0.93	1.39	1.99	-	-	-	-	80.2
4	3	0.67	1.12	1.70	2.24	-	-	-	-	78.9
5	0	0.51	0.93	1.33	1.73	2.27	-	-	-	83.7
5	3	0.50	0.67	1.12	1.70	2.24	-	-	-	82.0
6	0	0.51	0.93	1.17	1.47	1.83	2.33	-	-	85.8
6	3	0.50	0.67	1.12	1.37	1.70	2.23	-	-	84.9
7	0	0.12	0.93	1.15	1.41	1.73	2.07	2.53	-	87.5
7	3	0.49	0.67	0.93	1.12	1.39	1.70	2.23	-	87.1
8	0	0.49	0.69	0.93	1.15	1.41	1.73	2.07	2.53	89.3
8	3	0.49	0.67	0.93	1.12	1.39	1.70	2.03	2.49	89.1

Table 2: Optimum bandgap energies (in eV) and corresponding ultimate efficiency for solar cells with 1 to 8 junctions. The column 'Fixed' indicates the number of bandgaps that were fixed during the optimization of bandgaps, as is mentioned in chapter 4.1. If three bandgaps were fixed, these were fixed to the bandgap energies of Ge, c-Si and a-Si.

C.2 Efficiencies for Maximum Concentration

Junctions	Fixed	G1	G2	G3	G4	G5	G6	G7	G8	η (%)
1	0	1.12	-	-	-	-	-	-	-	45.1
2	0	0.70	1.52	-	-	-	-	-	-	60.4
3	0	0.52	1.12	1.82	-	-	-	-	-	67.8
3	3	0.67	1.12	1.70	-	-	-	-	-	67.2
4	0	0.51	0.93	1.39	2.01	-	-	-	-	72.7
4	3	0.67	1.12	1.70	2.26	-	-	-	-	71.5
5	0	0.51	0.93	1.35	1.75	2.29	-	-	-	75.7
5	3	0.50	0.67	1.12	1.70	2.26	-	-	-	74.2
6	0	0.51	0.93	1.19	1.53	1.91	2.41	-	-	77.4
6	3	0.49	0.67	1.12	1.39	1.70	2.25	-	-	76.5
7	0	0.51	0.93	1.15	1.41	1.73	2.09	2.55	-	79.3
7	3	0.51	0.67	1.12	1.39	1.70	2.03	2.49	-	78.6
8	0	0.51	0.71	0.93	1.15	1.41	1.73	2.09	2.55	81.0
8	3	0.51	0.67	0.93	1.12	1.39	1.70	2.03	2.49	80.7

Table 3: Optimum bandgap energies (in eV) and corresponding efficiency for solar cells with 1 to 8 junctions under maximum concentration and taking χ to be 1. The column 'Fixed' indicates the number of bandgaps that were fixed during the optimization of bandgaps, as is mentioned in chapter 4.1. If three bandgaps were fixed, these were fixed to the bandgap energies of Ge, c-Si and a-Si.

C.3 Efficiencies for No Concentration or Angular Restriction

Junctions	Fixed	G1	G2	G3	G4	G5	G6	G7	G8	η (%)
1	0	1.14	-	-	-	-	-	-	-	33.3
2	0	0.94	1.64	-	-	-	-	-	-	45.6
3	0	0.92	1.40	2.02	-	-	-	-	-	51.3
3	3	0.67	1.12	1.70	-	-	-	-	-	50.5
4	0	0.69	1.13	1.57	2.15	-	-	-	-	55.3
4	3	0.67	1.12	1.70	2.26	-	-	-	-	54.8
5	0	0.69	1.11	1.41	1.81	2.33	-	-	-	57.7
5	3	0.67	1.12	1.39	1.70	2.25	-	-	-	57.2
6	0	0.53	0.93	1.19	1.53	1.91	2.41	-	-	59.2
6	3	0.67	0.93	1.12	1.39	1.70	2.25	-	-	58.8
7	0	0.53	0.93	1.15	1.41	1.73	2.09	2.55	-	60.6
7	3	0.67	0.93	1.12	1.39	1.70	2.05	2.51	-	60.5
8	0	0.51	0.71	0.93	1.15	1.41	1.73	2.09	2.55	61.8
8	3	0.51	0.67	0.93	1.12	1.39	1.70	2.05	2.51	61.5

Table 4: Optimum bandgap energies (in eV) and corresponding efficiency for solar cells with 1 to 8 junctions with no concentration or angular restriction and taking χ to be 1. The column 'Fixed' indicates the number of bandgaps that were fixed during the optimization of bandgaps, as is mentioned in chapter 4.1. If three bandgaps were fixed, these were fixed to the bandgap energies of Ge, c-Si and a-Si.

D Semiconductor materials with abundant, non-toxic elements

Material	E_g (eV)	Direct (D) or Indirect (I) bandgap	Literature
PbS	0.5	D	[19, 20]
$CuFeS_2$	0.53	D	[19, 21]
Ge	0.66	I	[5, 19, 22, 23]
SiGe	0.67-1.12	I	[24]
Mg_2Ge	0.74	D	[19]
Mg_2Si	0.77	I	[19, 25]
β-$FeSi_2$	0.84-0.88	D	[26–28]
$CuGe_2P_3$	0.9		[19]
Cu_2SnS_3	0.91		[19, 29]
FeS_2	0.95	I	[30]
$PbSnS_3$	1.05		[29]
$Cu_2ZnSn(S_xSe_{1-x})$ (CZTS)	1.05-1.65	D	[31, 32]
c-Si	1.12	I	[19]
Cu_2S	1.2	D	[33, 34]
CuO	1.2	D	[26, 35]
CuN_3	1.2-1.9		[36]
CuN_3	1.2-1.9		[5]
a-SiGe:H	1.4-1.7	D	[37–39]
Zn_3P_2	1.4-2.2	D	[36]
$ZnSnP_2$	1.45		[19]
B	1.55		[19]
$CuGaSe_2$	1.68	D	[5]
a-Si:H	1.6-1.9	D	[5, 33, 40]
a-SiC	1.7-2.2	D	[5]
ZnP_2	1.7-2.2	D	[36]
AlB_{12}	1.9		[36]
Ca_2Si	1.9		[36]
SiP_2	1.9		[36]
Cu_2O	1.9-2.0	D	[35, 36]
$ZnSnP_2$	2.1		[19]
$ZnGeP_2$	2.2		[19]
GaP	2.24	I	[19, 41, 42]
3C-SiC [7]	2.38	I	[19, 43–45]
$ZnSiP_2$	2.3		[19]
$CuGaS_2$	2.38		[19]
AlP	2.45	I	[19]
$CuAlS_2$	2.5	I	[19, 46]

Table 5: Semiconductor materials with bandgaps between 0.5 and 2.5 eV, the relevant range for solar cell applications. These materials contain only abundant and non-toxic elements, which can be obtained in an economically feasible manner. A distinction is made between direct and indirect bandgap materials, insofar as information on this was present in the studied literature. Literature on each material is presented.

[7] SiC comes in many different crystal structures. 3C-SiC, also known as β-SiC or cubic SiC, has the best conductive properties and lowest bandgap. A disadvantage of 3C-SiC is that it is difficult to grow large wafers, although currently much work is being done on this subject. [43]